

# Analysis of $n^+p$ silicon junctions with varying substrate doping concentrations made under ultraclean processing technology

Herzl Aharoni<sup>a)</sup> and Tadahiro Ohmi

Department of Electronic Engineering, Faculty of Engineering, Tohoku University, Aza-Aoba, Aramaki, Aoba-ku, Sendai 980-77, Japan

Mauricio Massazumi Oka and Akira Nakada

Department of Electronic Engineering, Faculty of Engineering, Tohoku University, Aza-Aoba, Aramaki, Aoba-ku, Sendai 980-77, Japan and Laboratory for Electronic Intelligent Systems, Research Institute of Electrical Communications, Tohoku University, Aza-Aoba, Aramaki, Aoba-ku, Sendai 980-77, Japan

Yukio Tamai

Department of Electronic Engineering, Faculty of Engineering, Tohoku University, Aza-Aoba, Aramaki, Aoba-ku, Sendai 980-77, Japan

(Received 25 July 1996; accepted for publication 16 October 1996)

Using highly controlled ultraclean processing technology, marked improvements in  $n^+p$  Si junction quality are achieved presenting a theoretical significance. Boron-doped substrates with various boron doping concentrations  $N_s$  were As<sup>+</sup> implanted, forming the  $n^+$  junction sides. The diffusion ( $I_d$ ) and generation ( $I_{\text{gen}}$ ) currents, as well as the ideality and the generation factors, are significantly reduced, and bulk generation lifetimes are prolonged. Using Shockley–Read–Hall theory it is found that a deviation of the trapping centers energy ( $E_t$ ) from the midband-gap energy ( $E_i$ ) is responsible for the improvements. The experimental results show that  $|E_t - E_i|$  is a function of  $N_s$ , and that the  $I_{\text{gen}}/I_d$  ratio is significantly low. Accordingly, it is proposed that  $I_{\text{gen}}/I_d$  ratio should be regarded, under certain conditions, as a figure of merit for junction quality. It is concluded that the  $|E_t - E_i|$  deviation is related to the ultraclean processing technology used, due to the formation of new energy levels far from  $E_i$  and the suppression of introduction of new energy levels near  $E_i$ . Surface generation currents were found experimentally to be significant, and thus not negligible. Surface effects in general demonstrated similar trends to the bulk generation effects. © 1997 American Institute of Physics. [S0021-8979(97)06602-4]

## I. INTRODUCTION

Low value of reverse-bias current ( $I_R$ ) is an important indicator of a  $p$ - $n$  junction quality. Its value has the consequences of the performance of a wide array of semiconductor devices, such as solar cells, transistors, thyristors, etc. Among the four constituents of  $I_R$ , namely, diffusion ( $I_d$ ), tunneling ( $I_t$ ), bulk and surface generation ( $I_{\text{gen},b}$  and  $I_{\text{gen},s}$ , respectively) current components, the first two result from predesign considerations, for specific devices and applications, mainly through doping concentration. The space-charge region bulk and surface generation current components, on the other hand, which can be controlled to some extent, do not result from predesign considerations. They are parasitic in nature, and as such, their values are in principle, not unique even for a given group of junctions having nominally identical process type, crystal quality, doping concentrations, dimensions, and structure. This is because  $I_{\text{gen},b}$  and  $I_{\text{gen},s}$  depend on device process quality, in a very critical fashion. Essentially, the bulk and surface generation components present loss mechanisms that limit the performance of the above-mentioned devices, and they load the driving source without serving any useful purpose, while at the same time, enhancing circuit operation instabilities and increasing noise level. In nowadays integrated circuit (IC) technology,

$I_t$  is negligible at the doping concentrations commonly used. Accordingly, the attention in this work is focused on the  $I_d$ ,  $I_{\text{gen},b}$ , and  $I_{\text{gen},s}$ , where the sum of the last two components represent the overall generation current,  $I_{\text{gen}}$ . The ratio  $I_{\text{gen}}/I_d$  is experimentally shown in this work to present a measure of the junction quality.

In the present IC technology,  $I_{\text{gen}}$  exceeds  $I_d$  by far. Thus the  $I_{\text{gen}}/I_d$  ratio is high and can range from few tens to few hundreds. In such junctions (especially diffused junctions) the reverse-bias current  $I_R$  is thought to be practically equal to  $I_{\text{gen}}$ , and calculations of  $\tau_{\text{gen}}$ , the generation lifetime of carriers within the bulk space charge region is calculated directly from  $I_R$ , neglecting the surface current component.<sup>1</sup> While  $I_d$  in IC's is mainly determined by doping concentrations, the  $I_{\text{gen}}$  value can be suppressed in the same junction, in principle, by modifying fabrication quality, yielding greatly reduced  $I_{\text{gen}}/I_d$  ratios. This is achieved practically in this work by the suppression of foreign undesired contaminants unintentionally introduced into the  $p$ - $n$  junction structure during its processing. This suppression approach, which is in a class by itself, is made possible by using precisely controlled fabrication conditions in an ultraclean technology environment, in a high investment facility that was predesigned and built for future submicron ultra-large-scale integration (ULSI) research. In this facility a measurable and drastic reduction in the various contaminants in the laboratory atmosphere, gas storage tanks, gas delivery lines, and fabrication equipment, together with stringent Super Clean

<sup>a)</sup>On leave from the Department of Electrical and Computer Engineering, Ben-Gurion University of the Negev, Beer-Sheva 84105, Israel.

Room (SCR) laboratory practices are carefully maintained. Although all types of unwanted contaminants are maintained at low levels, this publication is concerned mainly with those undesired impurities, which, if introduced during processing into the junction, would form energy levels deep within the band gap, namely heavy metal atoms. Reduction of these atoms content is directly responsible for the very low  $I_{\text{gen}}/I_d$  ratios achieved in our experiments, together with meaningful improvements in other junction operational parameters, which will be listed in the sequel. The large magnitude of these improvements will be shown to be of theoretical significance. The processing steps and the technological environment that were utilized in fabricating the junctions in this work, will be briefly described in Sec. III.

A series of identical ion ( $\text{As}^+$ ) implanted  $n^+p$  junctions were made, with different substrate concentrations  $N_s$  ( $1.6 \times 10^{14} - 2.3 \times 10^{18} \text{ cm}^{-3}$ ), which served as the  $p$  side (boron doped) of the junction, in order to investigate this parameter's influence on device performance. The data indicate a strong influence of  $N_s$  on the junction parameters. Following the measurements of the current voltage ( $I$ - $V$ ) relations, fitting of the data to the routinely used double exponential expression for the  $I$ - $V$  characteristics of the forward bias recombination and diffusion current components, derived for the case where  $E_t = E_i$  and  $E_{st} = E_{si}$  (where  $E_{st}$  and  $E_{si}$  represent the trapping and intrinsic energy levels at the surface respectively), could not be achieved. The expected behavior of the above expression results, according to the Shockley-Read-Hall (SRH) theory,<sup>2,3,4</sup> a power of  $1/m$  (where  $m=2$  is the generation factor for  $E_t = E_i$  and  $E_{st} = E_{si}$ ) in the exponential term of the forward recombination current component. In addition, for the case of  $E_t = E_i$  and  $E_{st} = E_{si}$ , high  $I_{\text{gen}}/I_d$  is usually obtained. Surface currents are usually considered to be small with respect to overall reverse-bias currents  $I_R$ .<sup>1</sup> In such a case, indeed,  $I_R \approx I_{\text{gen},b}$  and  $\tau_{\text{gen}}$  can be calculated directly from  $I_R$ , and its value can be shown<sup>4,5</sup> to be equal to  $\tau_n$  the lifetime of the minority carriers outside the space-charge region (i.e.,  $\tau_{\text{gen}} = \tau_n$  in the case of one sided  $n^+p$  junctions). Finally, neglecting surface effects, the temperature dependence of the reverse-bias current should, in the  $E_t = E_i$  case, exhibit two slopes, one proportional to  $-E_g$  in the high temperature range, and the second, proportional to  $-E_g/2$  in the low temperature range, that represent the generation current.<sup>4,5</sup>

Our results exhibited significant deviations from all the above expected behavior, for the whole range of substrate concentrations. They can be summarized as follows:

- (1) Low  $I_{\text{gen}}/I_d$  ratios were obtained which were close to unity, the highest ratio being 7.2.
- (2) Surface current to junction (bulk) current ratios can reach significant values. Surface effects could not be neglected in the analysis.
- (3) Ideality ( $n$ ) and generation ( $m$ ) factors were close to unity, all over the current range. The slope in the low current regime, where the generation mechanism dominates in the case of  $E_t = E_i$ , never reached the value of  $1/2$ .
- (4) Generation lifetime of minority carriers within the bulk

space charge region is much longer than minority carrier lifetime outside the space charge region.  $\tau_{\text{gen}}/\tau_n$  ratios ranged from few tens to few thousands.

- (5) Temperature dependence of  $I_R$  in the low temperature range (where generation mechanism dominates in the case of  $E_t = E_i$ ) exhibited slopes significantly different from  $-E_g/2$ .

All the above deviations were found experimentally to be a function of the substrate doping concentration.

The objective of this work is to analyze in detail the performance of these super clean room (SCR) fabricated junctions, showing that the theoretical foundation for the above listed deviations can be obtained by the SRH theory using the basic equations where  $E_t \neq E_i$  and  $E_{st} \neq E_{si}$  conditions exist, with good agreement with the experimental data. This is done by resolving the reverse-bias current into its components, and examining the factors that govern each of them, and their contribution to the overall performance, as a function of  $N_s$ . Finally, an explanation is proposed which relates the experimental results to the ultraclean processing technology.

In Sec. II, a brief summary of the theory for  $E_t \neq E_i$  case for the bulk, and  $E_{st} \neq E_{si}$  case for the surface will be presented. In Sec. III the experimental part is outlined, describing the special features of the ultraclean technology used as well as junction fabrication details and parameters. In Sec. IV the data of the various junction operational parameters as a function of substrate doping concentration is given. In Sec. V those results are discussed in conjunction with the above outlined theory. Finally, conclusions (Sec. VI), followed by a summary (Sec. VII), are given.

## II. THEORY

The purpose of the following presentation is to quantitatively determine, directly from dc  $I$ - $V$  characteristics of a  $p$ - $n$  junction, the influence of the bulk and surface recombination/generation center concentrations  $N_t$  and  $N_{ts}$ , respectively, and their trapping energy levels  $E_t$  and  $E_{ts}$ , respectively, on the space-charge region bulk and surface recombination/generation currents, their temperature dependence, their generation factors  $m$ , their minority carrier lifetimes, and surface recombination velocities, all as a function of  $N_s$ . This is done in accordance with the SRH theory.<sup>2,3,5</sup> Since the large body of data that was generated in the experiments required a detailed treatment, the main expressions that will be used in the analysis are summarized for convenience.

In general, the bulk recombination current  $I_{\text{rec},b}$  of a  $p$ - $n$  junction operating under forward bias condition and the net recombination rate per unit volume per unit time  $U_b$  within the bulk space charge region are related by:

$$I_{\text{rec},b} = qA \int_0^W U_b(x) dx, \quad (1)$$

where  $q$  is the electron charge,  $A$  is the junction cross section,  $W$  the space charge region width and:<sup>4-6</sup>

$$U_b(x)$$

$$= \frac{\sigma_p \sigma_n v_{th} N_t [np - n_i^2]}{\sigma_n \left[ n + n_i \exp\left(\frac{E_t - E_i}{kT}\right) \right] + \sigma_p \left[ p + n_i \exp\left(\frac{E_t - E_i}{kT}\right) \right]}. \quad (2)$$

$n$  and  $p$  are the free carrier concentrations for electrons and holes, respectively,  $n_i$  is the intrinsic carrier concentration,  $v_{th}$  is the free carrier thermal velocity,  $T$  is the absolute temperature, and  $k$  is the Boltzmann constant. The simplifying assumptions used here are that within the bulk all the trapping centers ( $N_t$ ) possess the same energy level  $E_t$ , the capture cross sections for electrons ( $\sigma_n$ ) and holes ( $\sigma_p$ ) are both equal to  $\sigma$ , the recombination centers are evenly distributed all over the crystal volume, and that the  $pn$  product is constant all over the space-charge region<sup>4</sup> for a given forward bias condition. Band-gap narrowing is neglected as well. These approximations influence only the magnitude of the calculated results but not their trends. It can be shown that under the above approximations, the maximum value of  $U_b$  is given by:

$$U_{b,max} = \frac{1}{\tau_0} \frac{n_i (e^{qV/kT} - 1)}{2 \left[ e^{qV/2kT} + \cosh\left(\frac{E_t - E_i}{kT}\right) \right]}, \quad (3)$$

where from Eq. (2):

$$\tau_0 = \frac{1}{\sigma v_{th} N_t}. \quad (4)$$

In this work the influence of  $N_t$  and  $E_t$  is of major interest. In our  $n^+p$  junctions, the data obtained demonstrate that in the  $p$  side of the junctions,  $p_p \gg n_p$  and  $p_p \gg n_i \exp[(E_t - E_i)/kT]$  situation exists. In such a case, Eq. (2) can be approximated as  $U_b \approx \sigma_n v_{th} N_t (n_p - n_{p0})$ .<sup>4,7</sup> Accordingly, by definition,  $\tau_0$  represents in these junctions the minority carrier lifetime on the  $p$  side. Thus  $\tau_0 = \tau_n = 1/\sigma v_{th} N_t$ . Finally, under the approximation that maximum generation rate conditions (where  $n=p$ ) exist all over the space-charge region,<sup>4</sup> Eq. (1) becomes:

$$I_{rec,b} = qA W_F U_{b,max} = \frac{qA W_F n_i}{2 \tau_n} \frac{e^{qV/kT} - 1}{e^{qV/2kT} + \cosh\left(\frac{E_t - E_i}{kT}\right)}. \quad (5)$$

Equation (5), which presents the  $I$ - $V$  relation of the net bulk recombination component, was derived for forward bias conditions, where  $V = V_F > 0$ ,  $W = W_F$ , and  $np > n_i^2$ , within the bulk space-charge region. In reverse bias situation, where  $V = V_R < 0$ ,  $W = W_R$  and  $pn \ll n_i^2$ , within the bulk space charge region, the recombination is negligibly small and generation is dominant, yielding from Eq. (5) the reverse bulk generation current:

$$I_{gen,b} = - \frac{qA W_R n_i}{2 \tau_n \cosh\left(\frac{E_t - E_i}{kT}\right)}. \quad (6)$$

Using  $I_{gen,b} = Q_{gen}/\tau_{gen}$ , where  $Q_{gen} = qA W_R n_i/2$ , it follows from Eq. (6) that the generation lifetime of minority carriers within the bulk space charge region is given by:

$$\tau_{gen} = \tau_n \cosh\left(\frac{E_t - E_i}{kT}\right) \quad (7a)$$

and

$$I_{gen,b} = - \frac{qn_i W_R A}{2 \tau_{gen}}. \quad (7b)$$

From Eq. (7b) independent determination of  $I_{gen,b}$  leads to the calculation of  $\tau_{gen}$ , and by Eq. (7a) to the calculation of  $|E_t - E_i|$ . This is important since  $I_{gen,b}$  decreases as  $|E_t - E_i|$  increases [Eq. (6)], a fact that is of major interest in this work. Ideally,  $\tau_{gen}$  is expected to be independent of doping concentration,<sup>8,9</sup> since the space-charge region becomes depleted under reverse bias. Our data show, however, such a dependence, although a weak one. This is because  $E_t$  and  $N_t$  were experimentally found to be in this work, doping dependent for reasons which will be given in the discussion. Finally, according to Eq. (7a) large  $\tau_{gen}/\tau_n$  ratios indicate large deviations of  $E_t$  from  $E_i$ . This is confirmed by our data.

By analogy, a similar set of equations having identical form as Eqs. (1)–(6), describing the surface behavior can be written.<sup>4,10,11</sup> In these equations the same notations as in Eqs. (1)–(6) are used, possessing in addition the subscript  $s$  for surface. Accordingly,  $E_{st}$ ,  $E_{si}$ ,  $E_{sg}$ ,  $\sigma_{sn}$ ,  $\sigma_{sp}$ ,  $N_{st}$ ,  $n_s$ ,  $p_s$ , and  $U_s$  have the same meanings for the surface, as the parallel notations have for the bulk. As a result the surface current component due to the contribution of the surface generation centers at the silicon-oxide (S-O) interface, occupied by the junction periphery space-charge region area  $A_s$ , can be shown<sup>4,10,11</sup> to be

$$I_{gen,s} = q|U_s|A_s = \frac{1}{2}qn_i s A_s, \quad (8a)$$

where

$$U_s = -\frac{1}{2}n_i s \quad (8b)$$

and assuming  $\sigma_{sn} = \sigma_{sp} = \sigma_s$ :

$$s = \frac{s_0}{\cosh\left(\frac{E_{st} - E_{si}}{kT}\right)} \quad (8c)$$

and

$$s_0 = \sigma_s v_{th} N_{st}. \quad (8d)$$

In Eq. (8)  $U_s$  is the surface generation rate per unit area per unit time,  $N_{st}$  is the trapping centers concentration per unit area, and  $s$  is the surface recombination velocity (in cm/s) of minority carriers, all at the S-O interface. According to Eq. (8c),  $s$  becomes smaller as  $E_{st}$  deviates from  $E_{si}$ . From our data it can be inferred that similarly to the situation in the bulk  $|E_{st} - E_{si}|$  and  $N_{st}$  are substrate doping ( $N_s$ ) dependent. This will be discussed in Sec. V.  $s_0$  is the surface recombination velocity at the S-O interface for the  $E_{st} = E_{si}$  case, which results in [from Eq. (8c)] the highest value for  $s$ . According to Eq. (8a), independent measurement of  $I_{gen,s}$  can lead to the determination of  $s$  as a function of  $N_s$ . Using Eq. (8c), this dependence can provide a measure to the de-

viation of  $E_{st}$  from  $E_{si}$  as a function of  $N_s$ . This is important because as  $E_{st}$  deviates from  $E_{si}$ ,  $I_{\text{gen},s}$  decreases, according to Eq. (8).

The total reverse generation current  $I_{\text{gen}}$  is given by the sum of the bulk and surface generation components of Eqs. (7b) and (8a), respectively. The forward surface recombination current  $I_{\text{rec},s}$  due to recombination centers at the S–O interface is dependent exponentially on the forward voltage in a similar fashion as the bulk recombination current [Eq. (5)]. Accordingly, the total reverse generation and forward recombination currents  $I_{\text{gen}}$  and  $I_{\text{rec}}$ , respectively, are given by:<sup>4</sup>

$$|I_{\text{gen}}| = \frac{1}{2} q n_i \left( \frac{W_R A}{\tau_{\text{gen}}} + s A_{sR} \right), \quad (9a)$$

$$I_{\text{rec}} = \frac{1}{2} q n_i \left( \frac{W_F A}{\tau_{\text{gen}}} + s A_{sF} \right) (e^{qV_F/mkT} - 1). \quad (9b)$$

Changes in  $W$  in the bulk for forward and reverse bias are accompanied by parallel changes in  $A_s$  at the S–O interface. Accordingly  $A_s = A_{sR}$  for reverse bias and  $A_s = A_{sF}$  for forward bias. In Eq. (9b),  $m$  is the generation factor. Comparing Eq. (9b) to Eq. (5), and to expressions similar to Eq. (5) that can be written for the surface current using Eq. (8) it can be shown that in general  $m$  is dependent on  $E_t$ ,  $E_{st}$ ,  $N_t$ ,  $N_{st}$ ,  $\sigma_n$ ,  $\sigma_{sn}$ ,  $\sigma_p$ , and  $\sigma_{sp}$ . The generation factor equals 2<sup>4</sup> for the  $E_t = E_{st} = E_{si} = E_i$ ,  $\sigma_n = \sigma_p = \sigma$ , and  $\sigma_{sn} = \sigma_{sp} = \sigma_s$  case as can be seen from Eq. (5), and from a similar expression that can be written for the surface current. Otherwise  $m < 2$ , as is the case in this work. The expression in the square brackets in Eq. (9b), multiplying the exponential term is denoted  $I_{gf}$ , the generation current under forward bias conditions.

Generally, the  $N_t$  dependence on  $N_s$  can be described, in principle, by a power series. In this work only the first two terms are taken, as a practical approximation.<sup>12–15</sup> Accordingly:

$$N_t = N_{ti} + B N_s, \quad (10)$$

where  $B$  is a constant, and  $N_s$  is the substrate ( $p$  type) dopant concentration, which in our series of junctions constitute the low doped side of the junctions.  $N_t$  in Eq. (10) is the effective value of trapping centers concentration. That is, in addition to technological factors that induce certain amount of defects as described in the discussion,  $N_t$  is also determined by the position of the Fermi level enabling more of these defects to participate in the recombination process as  $N_s$  increased.<sup>16</sup> This is further discussed in Sec. V. Substituting Eq. (10) into Eq. (4) yields a very familiar experimental expression for the dependence of minority carrier lifetime on  $N_s$ , which was used by several researchers,<sup>12–14,17–19</sup> for both  $\tau_p$  and  $\tau_n$ , namely:

$$\tau_n = \frac{\tau_{ni}}{1 + \left( \frac{B}{N_{ti}} \right) N_s}, \quad (11)$$

where  $\tau_{ni} = 1/\sigma v_{th} N_{ti}$ , and  $N_{ti}$  are the lifetime and recombination centers concentration, respectively, at very low dop-

ing concentrations. For high doping concentrations  $\tau_n$  decreases proportionally to  $N_s^{-1}$ , due to the increase in the active defect concentration [Eq. (10)].

The temperature dependence of  $I_{\text{gen}}$  is determined mainly by  $n_i(T)$  and the hyperbolic expression of Eq. (6), and the parallel relation for the surface component of Eq. (8):

$$I_{\text{gen}} = -q \sqrt{N_v N_c} \left[ \frac{A W_R}{2 \tau_n} \frac{e^{-(E_g/2kT)}}{\cosh\left(\frac{E_t - E_i}{kT}\right)} + \frac{A_s s_0}{2} \frac{e^{-(E_{sg}/2kT)}}{\cosh\left(\frac{E_{st} - E_{si}}{kT}\right)} \right], \quad (12)$$

where  $N_v$  and  $N_c$  are the effective density of states in the valence and conduction bands, respectively. To get the general trend, then, for the case where  $E_t = E_{st}$ ,  $E_i = E_{si}$ ,  $E_g = E_{sg}$ , and  $|E_t - E_i| \gg kT$ , where  $T$  is the experimental temperature, yields the approximated result that the slope of  $I_{\text{gen}}$  in log scale versus  $1/T$  is proportional to  $-[E_g/2 + |E_t - E_i|]$ .<sup>5</sup> It can be seen that for  $E_t = E_i$  the expression is reduced to  $-E_g/2$ .

The diffusion component of the junction current used in this work is:<sup>4,5</sup>

$$I_D = I_d (e^{qV/kT} - 1), \quad (13a)$$

where

$$I_d = q A n_i^2 \left( \sqrt{\frac{D_n}{\tau_n}} \frac{1}{N_A} + \sqrt{\frac{D_p}{\tau_p}} \frac{1}{N_D} \right). \quad (13b)$$

$D_n$  is the electron diffusion constant and  $\tau_n$  is the electron lifetime in the  $p$  side.  $D_p$  and  $\tau_p$  are the same for holes in the  $n$  side.  $N_A$  and  $N_D$  are the  $p$  and  $n$  sides doping concentrations, respectively. The  $1/T$  dependence of  $I_d$  yields a slope proportional to  $-E_g$  at the high temperature through  $n_i^2(T)$ .

According to the above, the double exponential expression for the overall  $I$ - $V$  characteristics used in this work is:<sup>20</sup>

$$I = \frac{V - IR_s}{R_p} + I_{gf} (e^{q(V - IR_s)/mkT} - 1) + I_d (e^{q(V - IR_s)/kT} - 1). \quad (14)$$

$R_s$  and  $R_p$  in Eq. (14) are the equivalent series and parallel resistances of the junction, respectively, where  $R_p$  is connected directly across the ideal junction and  $R_s$  is the resistance between the junction and the terminals. The  $R_s/R_p$  ratio is assumed to be negligible when deriving Eq. (14) as verified by the experimental results. Finally, it is noted that Eq. (14) takes the standard form once  $E_t = E_i$  and  $E_{st} = E_{si}$  is substituted into the above equations, i.e., it results in  $m = 2$ ,  $\tau_{\text{gen}} = \tau_n = \tau_0$ ,  $I_{\text{gen},b} = q A W_R n_i / 2 \tau_0$ ,  $s = s_0 = \sigma_s v_{th} N_{st}$ , and the slope of the  $I_{\text{gen}}$  (log) vs  $1/T$  becomes proportional to  $-E_g/2$ .

Under reverse bias,  $R_p$  further increases and Eq. (14) becomes:

$$I_R = -[I_d + I_{\text{gen}}] = -[I_d + (I_{\text{gen},b} + I_{\text{gen},s})]. \quad (15)$$

Accordingly, calculating the junction overall reverse current density  $J_R$  by simply dividing the terminal current  $I_R$



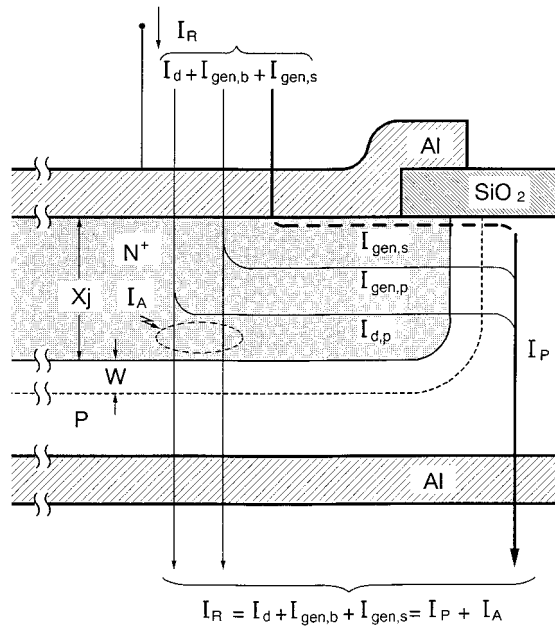


FIG. 1. A schematic description of various junction current paths.

by  $A$ , as sometimes done by various authors, is physically meaningless and can introduce a serious error to the analysis of this type. This is because  $I_R$  contain a peripheral component  $I_p$  (Fig. 1) which includes the surface current  $I_{gen,s}$  which flows via  $A_s$  and not through  $A$ . In addition  $I_p$  includes small fraction of the diffusion ( $I_{d,p}$ ) and bulk generation-current ( $I_{gen,p}$ ) of the junction as shown in Fig. 1, which schematically shows the various current paths. In this figure all the currents are assumed to flow at one side of the periphery, and they are shown as lumped components, for simplicity, while in reality they flow all around the periphery, in a distributed fashion. Similarly,  $I_{gen}$  [Eq. (9a)] and  $I_{rec}$  [Eq. (9b)] the overall generation and recombination currents, respectively, cannot be divided by  $A$  in order to find their current densities and for the same reasons, i.e., both contain surface components, which do not flow through  $A$ . The current  $I_A$  that flows through the junction cross section  $A$  is composed of the sum of  $I_d$  and  $I_{gen,b}$ . Accordingly the overall reverse current can be also expressed as the sum of the cross section (area) current and the peripheral current, i.e.,  $I_R = I_A + I_p$ . The peripheral current increases with  $L$  the length of the junction perimeter, at the periphery of the junction at the surface:

$$I_R = J_A A + J_p L. \quad (16)$$

The peripheral current density  $J_p$  in Eq. (16) has a dimension of current per unit length (A/cm).  $I_p$  and specifically its surface component  $I_{gen,s}$  can compose a significant portion of the overall reverse current as experimentally shown in this work and therefore cannot always be neglected. This problem becomes more severe as the junction area is decreased, since the  $L/A$  ratio increases, resulting an increase of the  $I_p$  fraction in  $I_R$  at the expense of  $I_A$  [Eq. (16)]. This bears a consequence on future ULSI devices since the scaling down of transistors dimensions can reduce the portion of the active (area) current that participates, for ex-

ample, in the amplification or switching action, in bipolar transistors, due to losses resulting from the increase in the surface generation current, which does not participate in the transistor action. Similar relations and remarks that were given for  $I_R$  apply for forward bias situation with the reversal of the current directions in Fig. 1. In this work, the contribution of  $I_p$  is investigated by producing on the same wafers a series of additional test junctions with varying  $L$  and keeping their area  $A_p$  the same. Dividing Eq. (16) by  $A = A_p$  yields:

$$I_R/A_p = J_A + J_p(L/A_p). \quad (17)$$

Plotting  $I_R/A_p$  vs  $L/A_p$ , for the above junctions, the resulting slope is  $J_p$  and the intersection with the vertical axis is  $J_A$ . The values of  $J_p$  and  $J_A$  obtained for the test junctions with the area  $A_p$  are the same for the junctions under investigation with area  $A$ , since both series were made simultaneously on the same wafers. This will be dealt with in detail in Sec. IV.

### III. EXPERIMENT

Ultraclean technology has been developed very extensively at Tohoku University and it is based on the conception that the process quality needed for future submicron ULSI manufacturing will require the complete elimination of contamination and process variations. The whole philosophy behind the ultraclean technology can be summarized in a few concepts: environmental clean, energy clean, magnetic clean, thermal clean, vibration clean, and process-variation clean.<sup>21,22</sup> In order to fulfill all these requirements, a number of technologies have been developed, some of the key ones being detailed below. Ultraclean gas system<sup>23-27</sup> has been achieved using tubing systems, gas cylinders, valves, and other components made of stainless steel with internal wall surface-electropolishing treatment that causes drastic reduction in the internal area and thus reduces outgassing as well as contamination adsorption and desorption (especially  $O_2$  and  $H_2O$  moisture). Most important, it drastically reduces the generation of particles, mainly heavy metals. The tubing lines and employed components were also carefully designed to eliminate deadzones that become source of particles due to the corrosion caused by the remaining gas. As a result, for the first time impurity levels of the order of ppb or even sub-ppb, instead of the usually reported ppm level, were attained. Table I compares the impurity levels obtained in the presently described gas system in comparison to typical values, taking  $N_2$  as an example.<sup>27</sup> Ultrapure water supply systems were designed not only to improve the water quality (reducing particles, bacteria, total organic content (TOC), dissolved oxygen, and  $SiO_2$ ) but also to continuously guarantee the same water quality obtained in the system output, at the user point.<sup>28</sup> Vibration control has been achieved by the use of pneumatically controlled high-performance active vibration removal unit and by minimizing vibration sources, which are motors used in the water and air circulation systems, by reducing their size and improving their efficiency, and the building itself, predesigned specifically for this laboratory by the use of appropriate construction techniques. The vibration measurement on the floor shows amplitudes of less than  $0.4 \mu m$  and less than  $0.15 \mu m$  for frequencies larger

TABLE I. Comparison of the impurity levels obtained in the gas system of the super clean room (SCR) of the Tohoku University compared to typical values.

Impurity	H <sub>2</sub> O (ppb)	CO <sub>2</sub> (ppb)	O <sub>2</sub> (ppb)	NO (ppb)	THC <sup>a</sup> (ppb)	Others (ppb)
SCR	1.8	<0.1	<0.1	<0.1	<0.1	<0.1
typical	<200	<10	1200	...	<50	...

<sup>a</sup>Total Hydro Carbon.

than 3 Hz and for frequencies between 3 and 10 Hz, respectively.<sup>25,29</sup> Elimination of static electricity and magnetic fields in the fabrication environment has been pursued.<sup>30,31</sup> Static electricity is kept below 6 V which is at least less than half of the average values usually reported, and much less than the maximum values that can reach locally to a typical value of 100 V or higher in usual clean rooms. Magnetic fields variations are kept below 1 mG eliminating their variation effects on processes that make use of electron or ion beams.<sup>30,31</sup> The presently described experiments were totally carried out in a facility built using all the above technologies, where the cleanliness defined as the number of particles with radii greater than 0.17  $\mu\text{m}$  is less than  $2 \times 10^{-6}/\text{ft}^3$ , in comparison to values of around 1–10/ $\text{ft}^3$  usually used in today's technology.<sup>32</sup>

The ultrahigh vacuum medium-current ion implanter employed in this experiment has a background pressure of  $10^{-10}$  Torr, and uses an ultraclean gas delivery system<sup>33,34</sup> for the ion source. Wafers are held by electrostatic chucks<sup>35</sup> from their back side. The vacuum chamber as well as the internal components of the system are made almost entirely of aluminum alloys and the inner surfaces are TiN coated to minimize outgassing. Plates made of Si are strategically positioned inside the implanter in order to minimize the amount of metal contaminants sputter-generated by the high energy ion beam allowing the concentration of metal contamination to be kept lower than  $10^{10}$  atoms/ $\text{cm}^2$ <sup>36</sup> as shown in Table II. It is important to notice that the detection limit of the total reflection x-ray fluorescence analysis (TRXRFA) equipment used in Table II is of the order of  $10^{10}$  atoms/ $\text{cm}^2$ . In other words, there is no detectable amount of metallic contaminant even after ion implantation.

Si wafers of  $p$  type doped with B, (100) orientation, grown by Cz and FZ methods were employed. The series includes FZ wafers with substrate concentrations of  $1.6 \times 10^{14}$ ,  $2.5 \times 10^{15}$ , and  $2.8 \times 10^{16} \text{ cm}^{-3}$ , and Cz wafers with concentrations of  $6.3 \times 10^{14}$ ,  $2.5 \times 10^{15}$ ,  $1.3 \times 10^{17}$ , and  $2.3 \times 10^{18} \text{ cm}^{-3}$ . These concentrations were determined by measuring the capacitance-voltage ( $C$ - $V$ ) characteristics of metal-oxide-semiconductor (MOS) capacitors fabricated using these wafers. After performing the RCA cleaning, 600-

nm-thick field oxide was initially formed by pyrogenic oxidation at 1000 °C. This oxide was etched from the wafer backside by buffered HF (BHF) and 200-nm-thick borosilicate glass (BSG) was deposited by atmospheric pressure chemical vapor deposition (APCVD) ( $\text{SiH}_4$ ,  $\text{O}_2$ , and  $\text{B}_2\text{H}_6$ ) at 400 °C. This BSG film was used as a source for the B diffusion, carried out at 1000 °C, in order to facilitate the ohmic contact at the wafer backside. After removing the BSG film, the active area was patterned on the top surface, forming a square geometry with area of  $A = 1 \times 1 \text{ mm}^2$ .  $\text{As}^+$  was implanted into the exposed bare silicon in the ultraclean ion implantation machine<sup>33,34,36</sup> at 25 keV with a dose of  $2 \times 10^{15} \text{ cm}^{-2}$ . Post-implantation annealing was carried out at 1000 °C in  $\text{N}_2$  ambient for 30 min, yielding  $x_j$  ranging from 0.245 to 0.362  $\mu\text{m}$  depending on  $N_s$ . 100-nm-thick oxide was deposited on the top surface by APCVD at 400 °C and 250-nm-thick Al was evaporated over it. Aluminum guard rings situated at a distance of 50  $\mu\text{m}$  from the junction periphery having a width of 40  $\mu\text{m}$  were patterned around the diodes in order to electrically isolate the individual diodes by forming an accumulation region through MOS capacitance action. 1- $\mu\text{m}$ -thick oxide was deposited at the top surface by APCVD at 400 °C and contact holes for the  $n^+$  side of the junctions, and for the guard rings were patterned over it. An alloy of Al/Si was then deposited by sputtering to the frontside and Al was evaporated to the backside of the wafer. Contact pads for the  $n^+$  side of the junctions and for the guard rings were patterned on the frontside. Finally, sintering in forming gas environment was carried out at 400 °C for 20 min. Additional set of junctions for the determination of peripheral current component  $I_p$  was made simultaneously on the same substrate, with identical processing conditions and sequence, including guard rings. Four different junctions were employed in each substrate, all having the same area ( $A_p = 0.0016 \text{ cm}^2$ ) but different perimeter  $L$ . The geometries used were square ( $400 \times 400 \mu\text{m}$ ) for the lowest perimeter ( $L = 1600 \mu\text{m}$ ) and comb-shaped patterns for the larger perimeters. As a result four ratios of  $L/A_p$  were obtained for these junctions, namely, 100, 200, 300 and  $400 \text{ cm}^{-1}$ . They will be referred to as the "peripheral junctions." Accordingly, in the following, a distinction should be made between

TABLE II. Metal concentration measured by TRXRFA (total reflexion x-ray fluorescence analysis) over the Si wafer before and after ion implantation (I/I).

Metal		Fe	Cu	Ni	Mn	Cr	Co	Zn	Ti
Concentration $\times 10^{10}$ (atoms/ $\text{cm}^2$ )	Before I/I	3.5	0.0	1.0	0.0	1.9	0.0	0.0	0.0
	After I/I	5.1	1.7	1.0	0.0	2.1	0.0	3.2	0.0

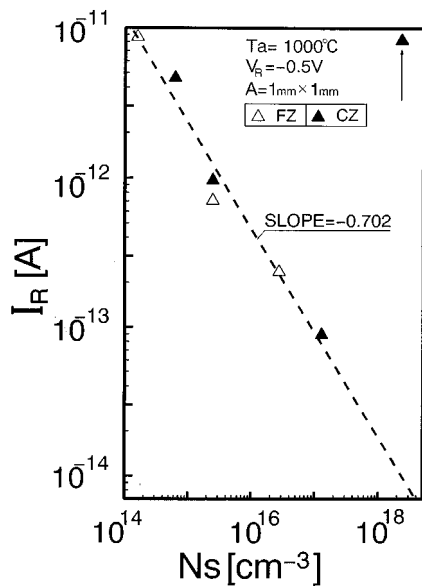


FIG. 2. Reverse bias current  $I_R$  at  $V_R = -0.5$  V, as a function of substrate dopant concentration,  $N_s$  ( $1 \times 1$  mm<sup>2</sup> junctions).

the main series of junctions with area of  $1 \times 1$  mm<sup>2</sup> which are the subject of this work, and the “peripheral junctions” used only to determine  $J_p$  and  $J_A$ , according to Eq. (17).

The data presented in the next section was measured in the computer controlled HP-4061 test system, under dark conditions, at 300 K, with  $-5$  V applied to the guard ring with respect to the substrate. The  $1 \times 1$  mm<sup>2</sup> junctions selected were the best in each wafer (i.e., the lowest  $I_R$ ). Special care was taken in determining the time interval between measurements of  $I$ - $V$  points at the very low current levels near the origin. This is needed due to the large charging time of the junction capacitance via the high impedance which exists at low currents (down to  $10^{-15}$  A). Our experience showed that otherwise large errors in the junction parameters information extracted from this current region may result. This is important in this work since  $R_p$  as well as generation parameters such as  $I_{gf}$ , and  $m$  are mainly determined from the low current region. As mentioned, these errors were all eliminated. The data presented below was fitted by the least square method.

#### IV. RESULTS

Figure 2 shows the reverse bias current  $I_R$  of the  $1 \times 1$  mm<sup>2</sup> junctions as a function of the substrate concentration  $N_s (= N_A)$ , measured at reverse bias of 0.5 V. Good fit to a straight line is obtained except for the  $2.3 \times 10^{18}$  cm<sup>-3</sup> substrate, where the current significantly deviates to a high value (indicated by an arrow). This is due to a high tunneling current component as verified by the low breakdown voltage and its negative temperature coefficient. Accordingly, this point deviates also in other relevant graphs in this work and will be indicated in each case. By fitting the measured forward bias characteristics of the  $1 \times 1$  mm<sup>2</sup> junctions to Eq. (14),  $I_d$ ,  $I_{gf}$ ,  $m$ ,  $R_s$ , and  $R_p$  were obtained, all as function of  $N_s$  as shown in Figs. 3 to 7. Two slopes appear in Fig. 3 for  $I_d$ . The straight line fitting for the low doping concentration

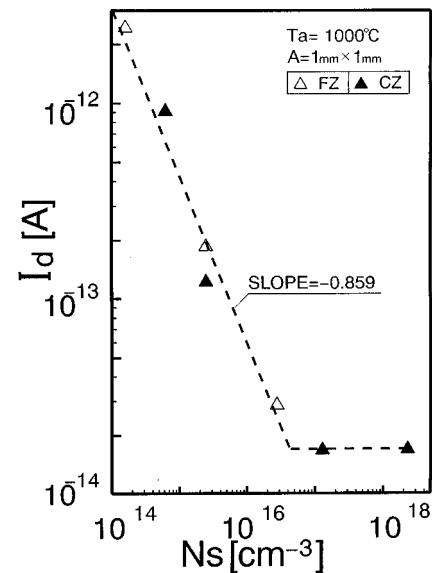


FIG. 3. Diffusion current  $I_d$  as function of substrate dopant concentration,  $N_s$  ( $1 \times 1$  mm<sup>2</sup> junctions).

range (up to  $10^{17}$  cm<sup>-3</sup>) indicates that the junctions can be regarded as one sided, where the  $As^+$  doped  $n^+$  side is a dominant current injector (electrons) under forward bias. Its slope indicates that  $\tau_n$  in the  $p$  side is decreasing with increasing  $N_s$ , as will be shown later. The slope at the high substrate concentration portion indicates that the  $p$  side injects, under forward bias, significant currents as well, in those junctions (holes to the  $n^+$  side), and that, accordingly, should be regarded as two sided junctions.  $I_{gf}$  in Fig. 4 exhibits a straight line fitting except for the tunneling junction. This is meaningful because it is noted that this point deviates only in the  $I_{gf}$  case, and not in the  $I_d$  case. This is because both  $I_{gf}$  and  $I_{tf}$ , the tunneling current, are the result of mechanisms that take place within the high field depletion

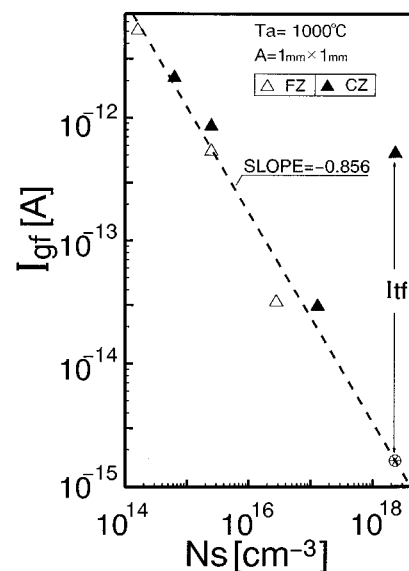


FIG. 4. Generation current component  $I_{gf}$  under forward bias, as a function of substrate dopant concentration ( $1 \times 1$  mm<sup>2</sup> junctions).

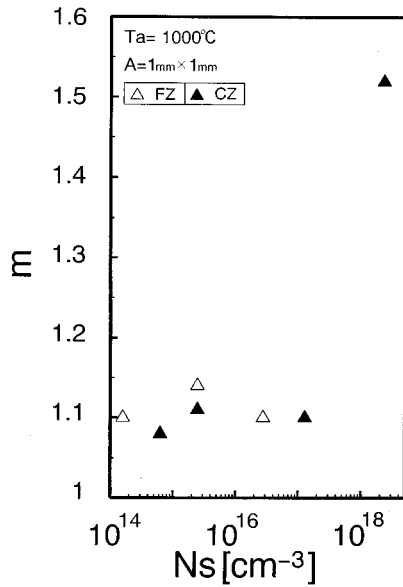


FIG. 5. Generation factor  $m$ , as a function of substrate dopant concentration  $N_s$  ( $1 \times 1$  mm<sup>2</sup> junctions).

region, while  $I_d$  is determined by the injection in the low field quasi-neutral zones, out of the junction space-charge region. In our case it is possible to resolve the generation and the tunneling components for this junction. The generation current for this substrate is approximated to lie on the straight line of  $I_{gf}$ , as indicated by the crossed circle in Fig. 4. In the sequel, this point, and not the deviated point will represent  $I_{gf}$  for this concentration in the data manipulation. The vertical distance from this point to the measured point represents  $I_{tf}$ , the tunneling current. The tunneling behavior in this junction will be described in detail separately.<sup>37</sup> The  $m$  values in Fig. 5 are close to unity (typically 1.1). No dependence of  $m$  on  $N_s$  could be observed. Similar behavior

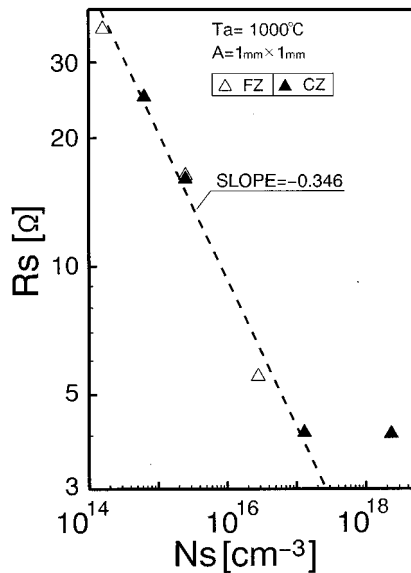


FIG. 6. Equivalent series resistance  $R_s$  as a function of substrate dopant concentration  $N_s$  ( $1 \times 1$  mm<sup>2</sup> junctions).

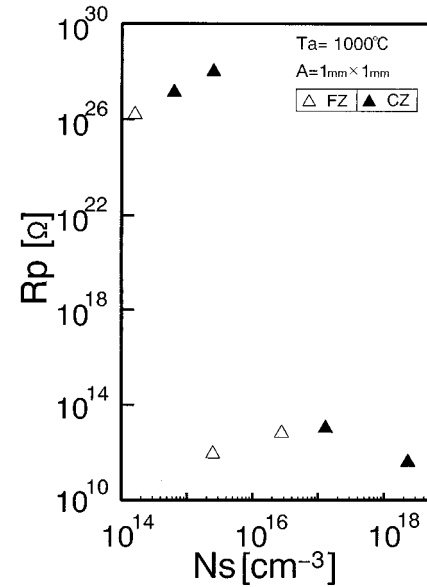


FIG. 7. Equivalent parallel resistance  $R_p$  as a function of substrate dopant concentration  $N_s$  ( $1 \times 1$  mm<sup>2</sup> junctions).

was found for the ideality factor  $n$  (not shown). The low values obtained for  $I_{gf}$  and  $m$ , hint that  $E_t \neq E_i$  and  $E_{st} \neq E_{si}$  situation might exist for these junctions. This will be addressed later on. Figure 6 shows that  $R_s$  is decreasing monotonically with increasing  $N_s$ . The slope indicates that  $R_s$  includes not only bulk resistivity, but other effects as well, such as contact and possibly high injection effects. While  $R_s$  exhibits monotonic behavior,  $R_p$  (Fig. 7), in contrast, exhibits a significant sharp drop in its value for  $N_s \geq 2.5 \times 10^{15}$  cm<sup>-3</sup>. The high values of  $R_p$  for  $N_s \leq 2.5 \times 10^{15}$  cm<sup>-3</sup> do not represent any physical significance except indicating that  $R_p$  is very high in this region. This is due to the fact that the currents in this  $R_p$  region are much below the  $10^{-15}$  A which is the measurement limit. The actual numbers for this region are higher. However, the sharp transition to the lower values, as well as the lower values of  $R_p$  ( $10^{11}$ – $10^{13}$  Ω) represent real effects. Such values are usually neglected, but as for the junctions in this work they will be shown to be of importance for the determination of the correct values of  $I_{gf}$  and  $I_d$ . Possible reasons for this  $R_p$  behavior will be given in the discussion.

In order to determine the surface current, the reverse current  $I_{Rp}$  (at  $V_R = -0.5$  V) of the four test structures termed “peripheral junctions” in the experimental section was measured at reverse bias of 0.5 V, and  $-5$  V applied to their guard rings. Figure 8(a) shows  $I_{Rp}$  as a function of  $N_s$  for the largest perimeter junction as an example. Figure 8(b) shows the plot of  $I_{Rp}/A_p$  vs  $L/A_p$  according to Eq. (17), for the junctions with  $N_s = 6.3 \times 10^{14}$  cm<sup>-3</sup> (Cz wafer) as an example. A good fitting to a straight line is obtained and the values of the peripheral current density ( $J_p$ ) and the cross section (area) current density ( $J_A$ ) are obtained for this junction from the slope and from the point where the dashed line cross the vertical axis, respectively. An increase in scattering of the data was noted as  $N_s$  increased. Figures 9 and 10 show the values of  $J_p$  (A/cm) and  $J_A$  (A/cm<sup>2</sup>) obtained by this way



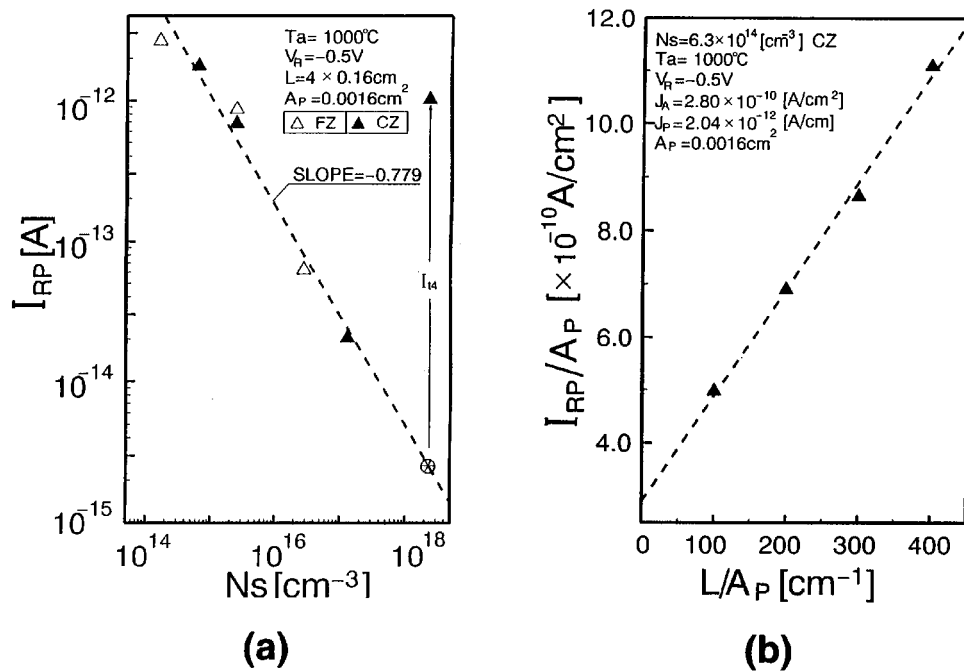


FIG. 8. (a) The reverse current  $I_{RP}$  ( $V_R = -0.5$  V) of the largest perimeter ( $L = 4 \times 0.16$  cm) peripheral test diode, as a function of substrate dopant concentration. (b) The  $I_{RP}/A_P$  ratio as a function of  $L/A_P$  for the four peripheral test diodes for the  $N_s = 6.3 \times 10^{14}$  cm $^{-3}$  Cz diodes.

for the whole range of  $N_s$ , of the peripheral junctions. These values of  $J_p$  and  $J_A$ , however, are the same for the  $1 \times 1$  mm $^2$  junctions as well, since as mentioned in Sec. III both junctions are fabricated on the same substrates and measured under the same conditions. Accordingly, the results obtained above for  $J_p$  and  $J_A$  are used in the following to determine  $I_p$  and  $I_A$  in the  $1 \times 1$  mm $^2$  junctions by multiplying  $J_p$  and  $J_A$  by  $L = 0.4$  cm, and  $A = 0.01$  cm $^2$ , respectively. Accordingly all the following figures (Figs. 11–22) are referred to the  $1 \times 1$  mm $^2$  junctions. In Figs. 9 and 10, it is noted that the

data points for the  $2.3 \times 10^{18}$  cm $^{-3}$  junction deviate from the fitted lines. This is mainly due to surface and bulk tunneling, respectively, as will be shown later on. The same point in Fig. 8(a) includes the combined tunneling current ( $I_{t4}$ ). Figure 11 presents the ratio of the peripheral currents  $I_p$  to the area currents  $I_A$  as a function of  $N_s$ . With the exception of the tunneling junction, the data separation of the Cz and FZ substrates in Fig. 11 clearly reveals the fact that could not be explicitly seen in Figs. 9 and 10, that is, in junctions made of

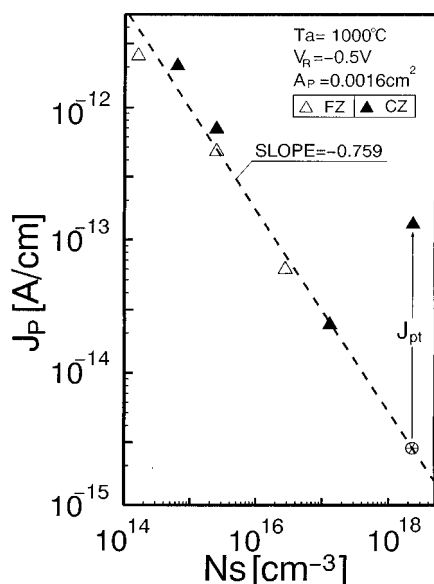


FIG. 9. The peripheral current density  $J_p$  obtained from the various slopes of the  $I_{RP}/A_P$  vs  $L/A_P$  of the peripheral test junctions as a function of  $N_s$ .

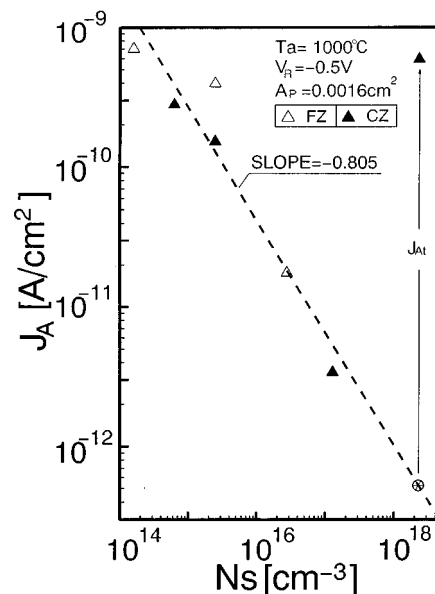


FIG. 10. The junction cross section (area) current density  $J_A$ , obtained from the intersection of the lines with the  $I_{RP}/A_P$  axis (vs  $L/A_P$ ) of the peripheral test junctions as a function of  $N_s$ .

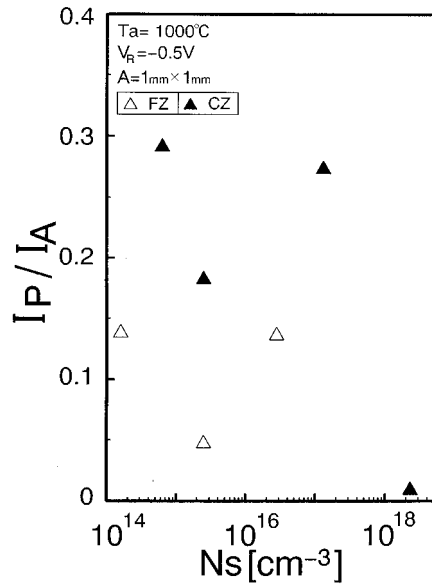


FIG. 11. The ratio of the peripheral current to the cross section current as a function of  $N_s$  ( $1 \times 1$  mm<sup>2</sup> junctions).

Cz crystals the  $I_p/I_A$  ratio (20%–30%) is significantly higher than those made in FZ crystals (5%–15%), depending on  $N_s$ . This is despite the fact that both surfaces were treated simultaneously by the same process. This result can be understood, bearing in mind that the quality of FZ crystals are superior to those of Cz crystals due to the lower oxygen content. As discussed in Sec. V, oxygen gives rise to generation/recombination centers. This is true for both bulk and surface. Such high values of  $I_p$  cannot be neglected if  $\tau_{\text{gen}}$  and  $|E_t - E_i|$  as well as  $J_{\text{gen},b}$  needed to be determined, even for junctions as large as  $1 \times 1$  mm<sup>2</sup>. Paradoxically, the above high ratios arise due to the higher quality of device processing which improves the bulk properties more than the

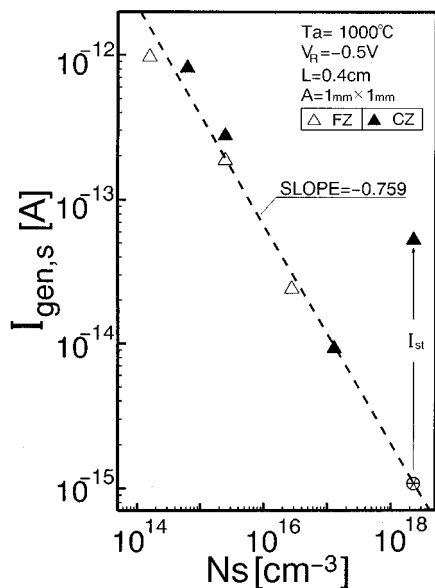


FIG. 12. The surface generation current as a function of  $N_s$  ( $1 \times 1$  mm<sup>2</sup> junctions).

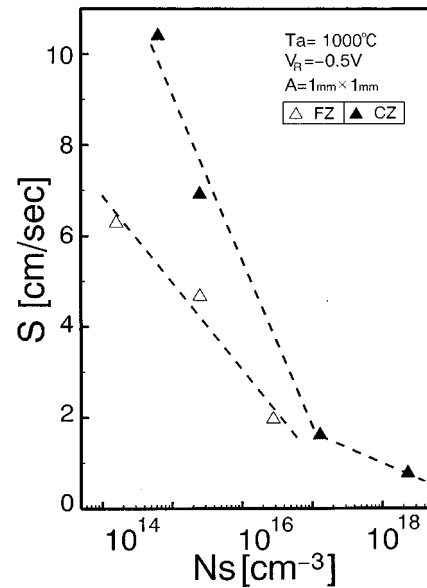


FIG. 13. Surface recombination velocity as a function of substrate doping concentration ( $1 \times 1$  mm<sup>2</sup> junctions).

surface properties which, in the junctions under discussion, are largely determined by the oxide–silicon interface properties. As mentioned, the increase in  $I_p/I_A$  ratio becomes a severe problem in ultra-large-scale integrated (ULSI) devices where  $L/A$  increases due to the scaling down of device areas. The peripheral currents are recently discussed in the literature<sup>38–40</sup> where the authors attribute the large  $I_p$  found in their junctions to field emission effects.

$I_p$  is composed of (Fig. 1)  $I_{\text{gen},s}$ ,  $I_{d,p}$ , and  $I_{\text{gen},p}$ . The relative contributions of each of these components to  $I_R$  can be estimated by a simplifying assumption that  $J_{d,p}$  and  $J_{\text{gen},p}$  are the same as in the rest of the area  $A$ , then,  $I_R \approx (J_d + J_{\text{gen},b})A + (J_d + J_{\text{gen},b})Lx_j + I_{\text{gen},s}$ . The last two terms represent  $I_p$  and the first,  $I_A$ . Since the second term in our junctions (where  $A \gg Lx_j$  situation exists) is much smaller than the first one, and since  $I_p/I_A$  is high (Fig. 11) it implies that in this case practically  $I_p \approx I_{\text{gen},s}$ . This will be quantitatively verified later on. Figure 12 represents  $I_{\text{gen},s}$  ( $=J_p \times 0.4$  cm) as a function of  $N_s$ . Caution should be exercised when, unlike in this case, very small area junctions are analyzed where  $A$  becomes closer to the junction side wall area  $Lx_j$ . In such a case the above approximation may not be valid. Two points arise from the above. The first regards the deviation of the  $2.3 \times 10^{18}$  cm<sup>-3</sup> data point in Figs. 9 and 12. Since  $I_p \approx I_{\text{gen},s}$ , this deviation in both figures is mainly due to surface tunneling resulting from the high doping concentration in both sides of this junction. The value of the surface tunneling current  $I_{st}$  can be estimated by assuming that the value of the surface generation current density for this junction is on the fitted line of Fig. 12 as indicated by the crossed circle. In the following this point will represent  $I_{\text{gen},s}$  for this junction. The vertical distance between this point to the measured data point is the surface tunneling current  $I_{st}$ . The second point regards the calculation of  $s$  by Eq. (8a) assuming  $I_{\text{gen},s} = I_p$ , where  $A_s$  is the area of the surface depletion region around the periphery of the  $1 \times 1$  mm<sup>2</sup> junctions. Fig-

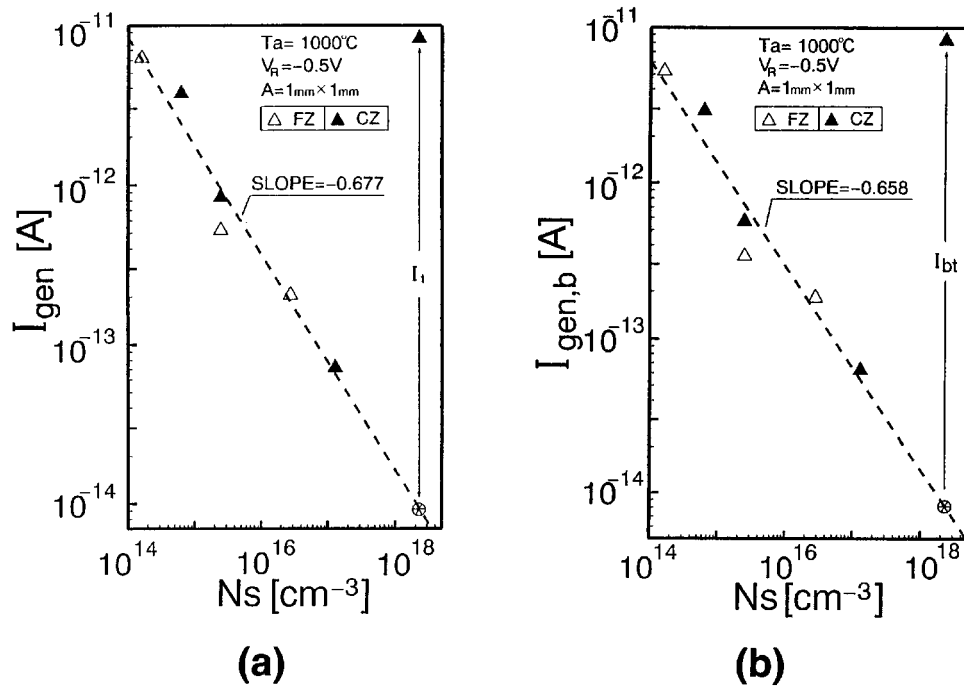


FIG. 14. (a) Overall reverse generation current  $I_{\text{gen}}$  as a function of  $N_s$  ( $1 \times 1 \text{ mm}^2$  junctions). (b) Bulk generation current component  $I_{\text{gen},b}$  as a function of  $N_s$  ( $1 \times 1 \text{ mm}^2$  junctions).

ure 13 presents the surface recombination velocity as a function of  $N_s$ . Again, as in the case of Fig. 11, the values of  $s$  for the FZ and Cz crystals are different for the same reasons. It is noted that  $s$  decreases with increasing  $N_s$ , unlike previously published data, where surface recombination velocity for  $p$ -type silicon demonstrated only moderate changes up to

the  $10^{16} \text{ cm}^{-3}$  doping concentrations and then an increase at higher concentrations.<sup>11</sup> This trend reversal of the surface recombination velocity is of principal significance and will be referred to in the discussion.

According to Eq. (15) the value of the total reverse generation current  $I_{\text{gen}}$  is calculated by subtracting  $I_d$  from  $I_R$ .

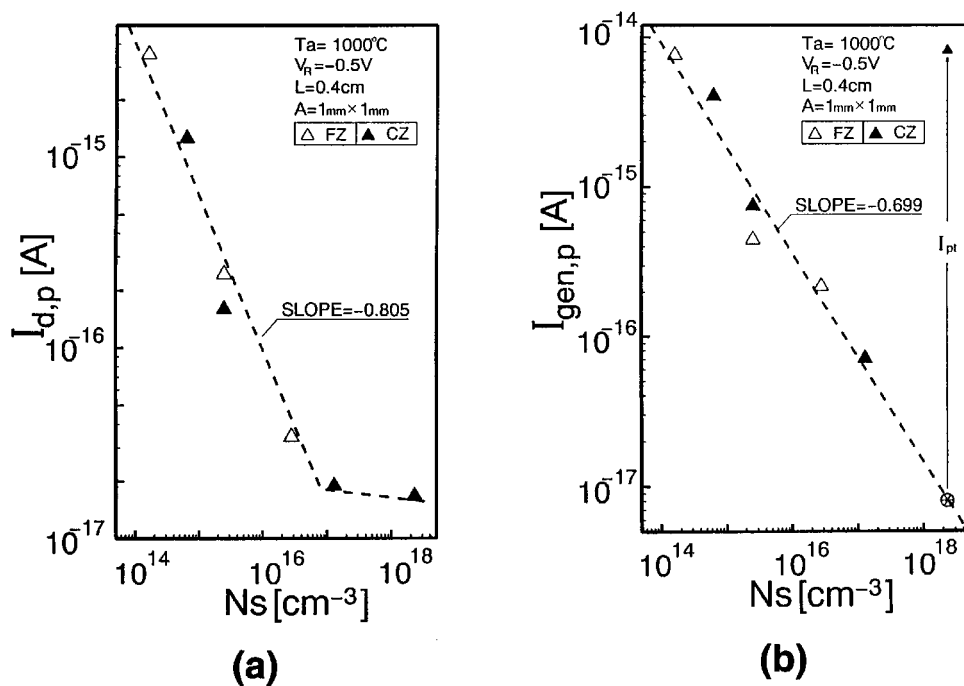


FIG. 15. (a) The peripheral (lateral) diffusion current component  $I_{d,p}$  as a function of  $N_s$  ( $1 \times 1 \text{ mm}^2$  junctions). (b) The peripheral (lateral) generation current component  $I_{\text{gen},p}$  as a function of  $N_s$  ( $1 \times 1 \text{ mm}^2$  junctions).

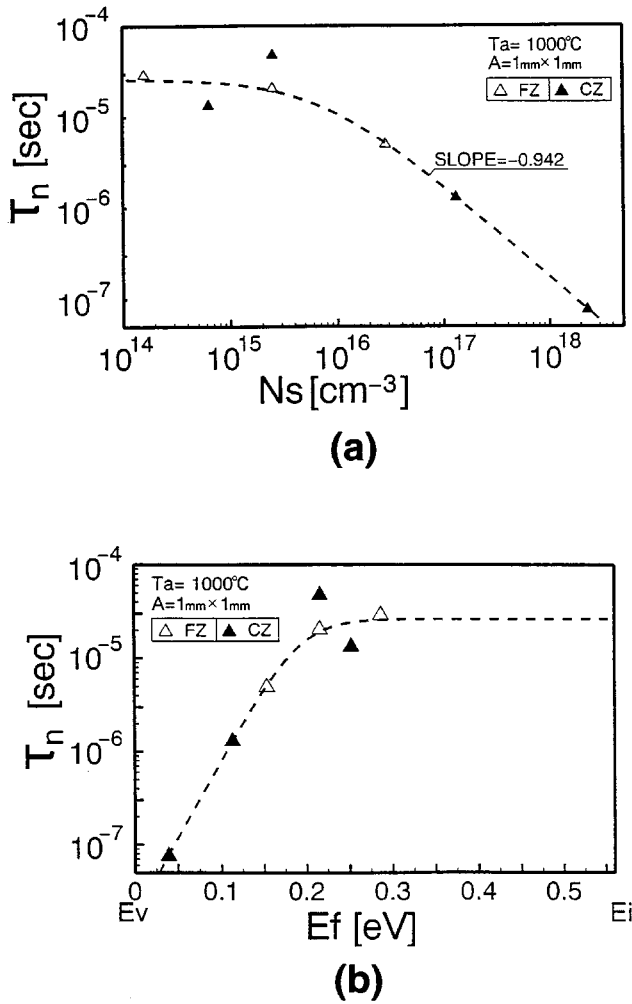


FIG. 16. (a) Minority carrier lifetime  $\tau_n$  of electrons in the  $p$  substrate as a function of substrate dopant concentration,  $N_s$  ( $1 \times 1$  mm<sup>2</sup> junctions). (b) Minority carrier lifetime  $\tau_n$  as a function of substrate Fermi level ( $1 \times 1$  mm<sup>2</sup> junctions).

The value of the reverse bulk generation current component  $I_{\text{gen},b}$  is obtained by subtracting  $I_{\text{gen},s}$  from  $I_{\text{gen}}$ . Figures 14(a) and 14(b) present  $I_{\text{gen}}$  and  $I_{\text{gen},b}$ , respectively, as a function of  $N_s$ . Again, in both cases the value of the  $2.3 \times 10^{18}$  cm<sup>-3</sup> data deviates from the fitted straight line. This deviation in Fig. 14(b) is due to the existence of bulk tunneling effect. The data point in Fig. 14(a) deviated due to the combined surface (Fig. 12) and bulk [Fig. 14(b)] tunneling components  $I_t = I_{bt} + I_{st}$ . In both cases the values of  $I_{\text{gen}}$  and  $I_{\text{gen},b}$  for the tunneling junction are approximated to lie on the fitted straight lines (crossed circles). In the following these points will represent  $I_{\text{gen}}$  and  $I_{\text{gen},b}$  for the respective  $2.3 \times 10^{18}$  cm<sup>-3</sup> junctions. The tunneling current in each case ( $I_t$  and  $I_{bt}$ , respectively), are determined as the vertical distance from the fitted straight line to the measured data point for this concentration. The tunneling current of Fig. 14(b) is responsible for the deviation of the  $2.3 \times 10^{18}$  cm<sup>-3</sup> data point in Fig. 10. The area current density  $J_A$  is composed (Fig. 1) of  $J_d$  and  $J_{\text{gen},b}$ . Since  $I_d$  (Fig. 3) does not have any tunneling component the only contribution of tunneling to  $J_A$  in Fig. 10 comes from Fig. 14(b). Finally, the contribution of

the two peripheral current components, namely  $I_{d,p}$  and  $I_{\text{gen},p}$  are crudely estimated assuming for simplicity that their current densities are the same as in the junction area. Figure 15(a) presents the lateral diffusion component ( $J_d L x_j$ ) and Fig. 15(b) represent the lateral generation component ( $J_{\text{gen},b} L x_j$ ) both as a function of  $N_s$ . Comparing the results to Fig. 12 it can be seen that  $I_{\text{gen},s} \gg I_{d,p}$ , and  $I_{\text{gen},s} \gg I_{\text{gen},p}$  situation exists, for about two orders of magnitude, verifying that in these junctions  $I_p \approx I_{\text{gen},s}$ . In Fig. 15(b) it can be seen that tunneling component exists, as expected.

According to Eq. (7a), in order to find  $|E_t - E_i|$ ,  $\tau_n$  and  $\tau_{\text{gen}}$  should be determined. This is addressed now. The values of  $\tau_n$  for the five one sided junctions of the high slope portion of Fig. 3 are obtained by the first term in Eq. (13b) which dominates over the second term in this  $N_s$  range. The values of the respective  $N_t$  were then calculated from Eq. (4) for these five junctions and were fitted to Eq. (10), yielding  $N_t = 3.8 \times 10^{12} + 5.64 \times 10^{-4} N_s$  [cm<sup>-3</sup>]. For estimation purpose, the  $N_t$  values for the remaining two sided junctions ( $N_s = 1.3 \times 10^{17}$  and  $2.3 \times 10^{18}$  cm<sup>-3</sup>) were assumed to be on the same straight line and their  $N_t$  values were calculated accordingly. Then, the respective  $\tau_n$  values for these two junctions were calculated from Eq. (4). The validity of using Eq. (4) for our junctions is dealt with in the sequel. The above procedure is based on the fact that Eq. (4) and Eq. (10) lead to Eq. (11), which is a well-established experimental dependence for  $\tau_n$ .<sup>12-14,17-19</sup> Figure 16(a) shows the  $\tau_n$  dependence on  $N_s$  with  $\tau_{ni} = 2.63 \times 10^{-5}$  s, which gave the best fit. The slope at the high concentration region of Fig. 16(a) indicates that  $\tau_n$  is inversely proportional to  $N_s$  as given by Eq. (11). This equation provides the lifetime due to phonon assisted recombination only, and does not include Auger recombination process that may take place in the vicinity of  $10^{18}$  cm<sup>-3</sup> dopant concentration. This will be referred to in the discussion. Figure 16(b) shows  $\tau_n$  as a function of the respective substrate Fermi levels which dominates  $\tau_n$ <sup>16</sup> as discussed in Sec. V.

$\tau_{\text{gen}}$  is calculated from  $|I_{\text{gen},b}|$  for all the junctions using Eq. (7b). The results are plotted in Fig. 17(a) which shows a weak dependence of  $\tau_{\text{gen}}$  on  $N_s$ , namely  $\tau_{\text{gen}} = 1.5 \times 10^{-6} N_s^{0.186}$  s. The ratio  $\tau_{\text{gen}}/\tau_n$  is shown in Fig. 17(b). This ratio is needed in order to determine  $|E_t - E_i|$  by Eq. (7a). It is interesting to note that despite the scattering in  $\tau_{\text{gen}}$  [Fig. 17(a)],  $\tau_{\text{gen}}/\tau_n$  [Fig. 17(b)] is relatively "smooth" as a function of  $N_s$  because the scattering in  $\tau_n$  and  $\tau_{\text{gen}}$  are canceled out. The  $\tau_{\text{gen}}/\tau_n$  ratio increases significantly with  $N_s$ , ranging from 25 to 1746 for dopant concentrations from  $1.6 \times 10^{14}$  cm<sup>-3</sup> to  $1.3 \times 10^{17}$  cm<sup>-3</sup>. The value of this ratio obtained for the tunneling junction is exceptionally high ( $5.54 \times 10^4$ ). Remembering that for  $E_t = E_i$  junctions,  $\tau_{\text{gen}}/\tau_n = 1$  [Eq. 7(a)], the result clearly shows that the influence of the deviation of  $E_t$  from  $E_i$ .  $|E_t - E_i|$  is now calculated for each substrate concentration junctions from this ratio by Eq. 7(a) and the results are plotted in Fig. 18. Again, only a small scattering is obtained despite the scattering in  $\tau_{\text{gen}}$ , due to the well behaved  $\tau_{\text{gen}}/\tau_n$  ratio. Figure 18 shows that as  $N_s$  increases,  $E_t$  deviates further from  $E_i$ . Possible explanation for this will be given in Sec. V. Similar arguments can be made for  $|E_{st} - E_{si}|$  at the S-O interface. Using the data of Fig. 13 it

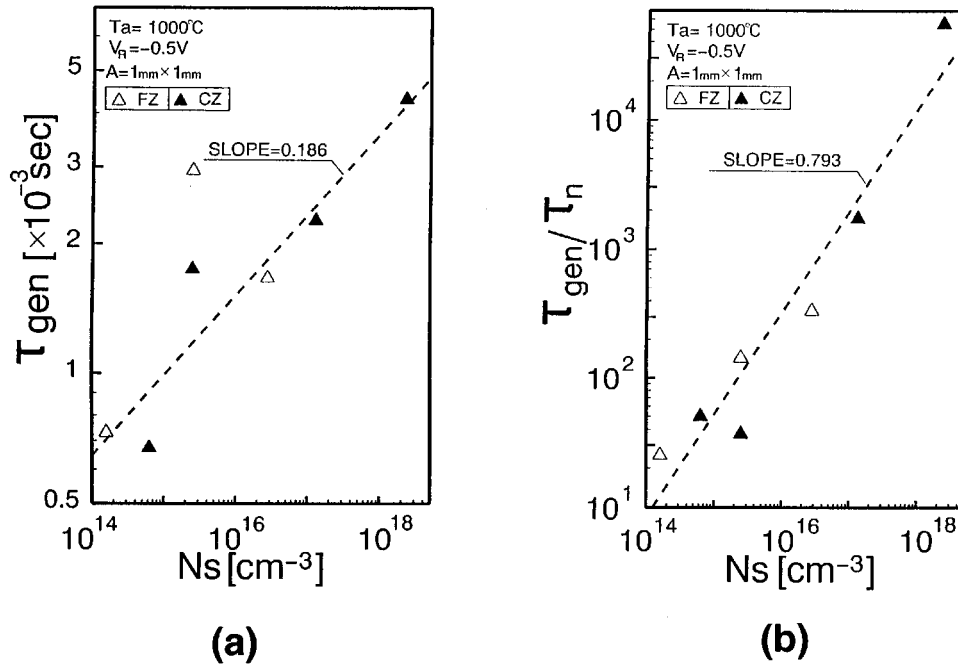


FIG. 17. (a) Generation lifetimes of the reverse biased junctions as a function of  $N_s$  ( $1 \times 1$  mm<sup>2</sup> junctions). (b) The ratio of depletion region lifetime to minority carrier lifetimes at the neutral zones of the junctions as a function of  $N_s$  ( $1 \times 1$  mm<sup>2</sup> junctions).

will be qualitatively shown in the discussion that  $E_{st}$  also deviates from  $E_{si}$ , as  $N_s$  increases.

In Sec. II  $\tau_n$  was equated to  $\tau_0$  [ $=1/\sigma v_{th} N_t$ , Eq. (4)] under a given approximation. The validity of the above approximation is shown now for our junctions. Figure 19(a) shows  $n_i \exp[|E_i - E_t|/kT]$  as a function of  $N_s (= p_p)$ . It is evident that for all the junctions under discussion, a situation where  $N_s \gg n_i \exp[|E_i - E_t|/kT]$  exists, as was required in Sec. II,<sup>4,7</sup> when  $\tau_n$  was equated to  $1/\sigma v_{th} N_t$  [from Eq. (2)]. Depending on the doping concentration,  $p_p$  exceeds the con-

centration of holes in the trapping centers by orders of magnitude. This is more conveniently demonstrated by Fig. 19(b) where the results show that the  $|E_i - E_F| > |E_i - E_t|$  situation exists for all the junctions, indicating that most of the trapping centers above  $E_F$  in the  $p$  side (substrate) are filled with holes. Accordingly,  $\tau_n$  in these junctions is dominated by the position of  $E_F$ ,<sup>16</sup> which is closer to  $E_v$  than  $E_t$ , which therefore, do not determine  $\tau_n$  for the junctions under discussion. As a result  $\tau_n$  is determined by the dependence of  $N_t$  on  $N_s$  only [Eq. (10)] which leads to Eq. (11). This will be further discussed in Sec. V.

The ratio of  $I_{gen}/I_d$  is given in Fig. 20. Two things are noted from the measured data. The first is the very small ratios obtained, ranging from less than unity to less than 7.2, and the second, that a maximum exists. This ratio is significantly smaller than that obtained for junctions where  $E_t = E_i$  and  $E_{st} = E_{si}$  situation exist (mainly in diffused junctions made using current technology clean room), which exhibit ratios ranging from few tens to few hundreds. These small ratios in Fig. 20 therefore present marked improvement which was achieved by the deviation of  $E_t$  from  $E_i$  and  $E_{st}$  from  $E_{si}$ , a fact that reflects on the junction quality. The shape of this dependence on  $N_s$  can be understood from Figs. 3 and 14(a). At the low  $N_s$  region,  $I_d$  decreases at a faster rate than  $I_{gen}$  while maintaining  $I_d < I_{gen}$ , resulting an increase in this ratio with  $N_s$ . At the high  $N_s$  region, this ratio decreases because  $I_{gen}$  continues to decrease, while  $I_d$  changes the slope due to the addition of the significant  $p$  side injection, causing an almost constant  $I_d$ . The contribution of bulk generation current  $I_{gen,b}$  and the surface generation current  $I_{gen,s}$  to the overall ratio of Fig. 20 are presented separately in Figs. 21(a) and 21(b), respectively. The results clearly show that the ratio of Fig. 20 is determined mainly by

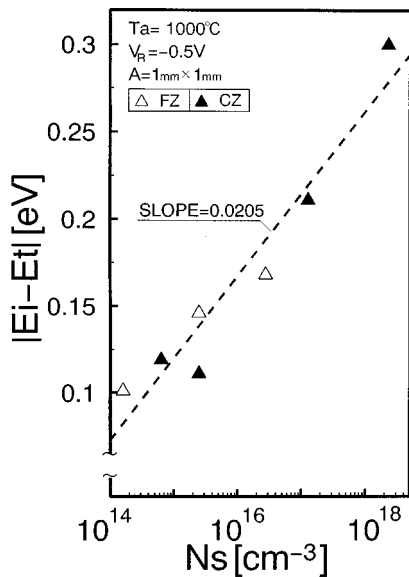


FIG. 18. The absolute value of the deviation of the trapping centers energy  $E_t$ , from mid-band-gap energy  $E_i$ , as a function of substrate dopant concentration  $N_s$ .



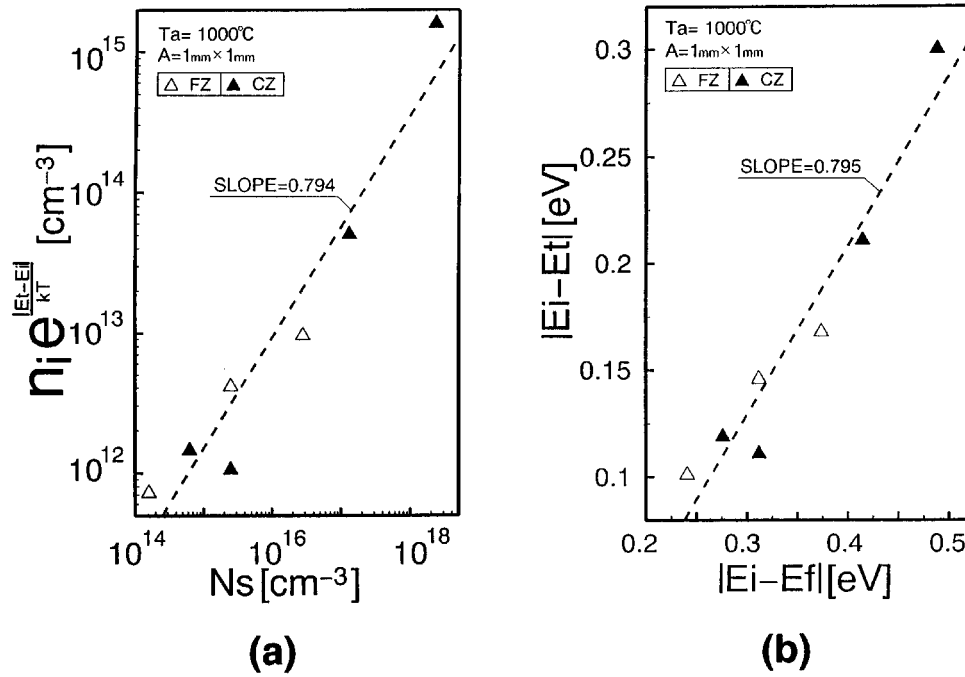


FIG. 19. (a)  $n_i \exp[(E_t - E_i)/kT]$  as a function of  $N_s$  ( $1 \times 1$  mm<sup>2</sup> junctions). (b)  $|E_t - E_i|$  as a function of  $|E_i - E_f|$ . An indication that in these junctions  $\tau_n$  is dominated by  $E_F$  and not by  $E_i$  ( $1 \times 1$  mm<sup>2</sup> junctions).

the bulk generation component. Both curves of Fig. 21 preserve the shape of Fig. 20, for similar reasons. The dashed lines of Figs. 20 and 21 represent the fitting done by using Eqs. 7(b), 8(a), 9(a), and 13(b). The values of  $s$ ,  $\tau_{\text{gen}}$ , and  $\tau_n$  in those equations were taken from the fitted values of Figs. 13, 16, and 17(a), respectively.  $D_n$  as a function of  $N_s$  was obtained from mobility data using  $D/\mu = kT/q$ .

A representative example for reverse current temperature dependence is given in Fig. 22 for junction made on Cz

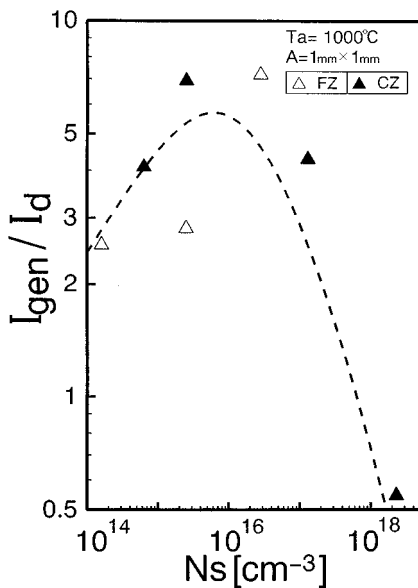


FIG. 20. Ratio of reverse overall generation current  $I_{\text{gen}}$  to the diffusion current  $I_d$ , as a function of substrate dopant concentration  $N_s$  ( $1 \times 1$  mm<sup>2</sup> junctions).

substrate with  $N_s = 2.5 \times 10^{15}$  cm<sup>-3</sup> boron concentration. Two slopes are observed, however neither exhibits the expected activation energy of  $-E_g$  and  $-E_g/2$  which would occur if  $E_t = E_i$  and  $E_{st} = E_{si}$  situation existed. This is probably because the slopes in these junctions do not purely represent the respective diffusion and generation regimes, since in these junctions relatively high surface current exists. According to Eq. (12) this can give rise to the deviation from  $-E_g/2$  as noted in the low temperature region where  $1000/T = 3-4$ , where  $I_{\text{gen},b}$  usually dominates (in the  $E_t = E_i$  case). The absolute value of the activation energy for the higher temperatures in the case of Fig. 22 is only about the band-gap energy. From Eq. (12) it is clear why  $|E_t - E_i|$  cannot be evaluated in our case by the slope of  $I_R/n_i$  as a function of  $1000/T$  as was suggested by Schroder.<sup>1</sup> In his junctions as well in other published cases this approach was possible, since  $I_{\text{gen}}/I_d$  was very high, and surface current was neglected so that the low temperature regime presented practically the pure bulk generation current ( $I_R \approx I_{\text{gen},b}$ ). As a result a new method should be devised for the determination of  $|E_t - E_i|$  by temperature measurements in future high quality junctions which is capable to resolve  $I_{\text{gen},b}$  as a function of  $T$ . Finally, as  $|E_t - E_i|$  increases, the slope of the low temperature region should approach that of the high temperature region. This was indeed observed for both the Cz and FZ junctions at the low substrate concentrations. However, this trend was reversed for  $N_s > 2.8 \times 10^{16}$  cm<sup>-3</sup> for both Cz and FZ substrates. This phenomena is not understood and it is still under investigation.

## V. DISCUSSION

The experimental results clearly demonstrated that the bulk depletion region generation parameters, namely,  $\tau_{\text{gen}}$ ,

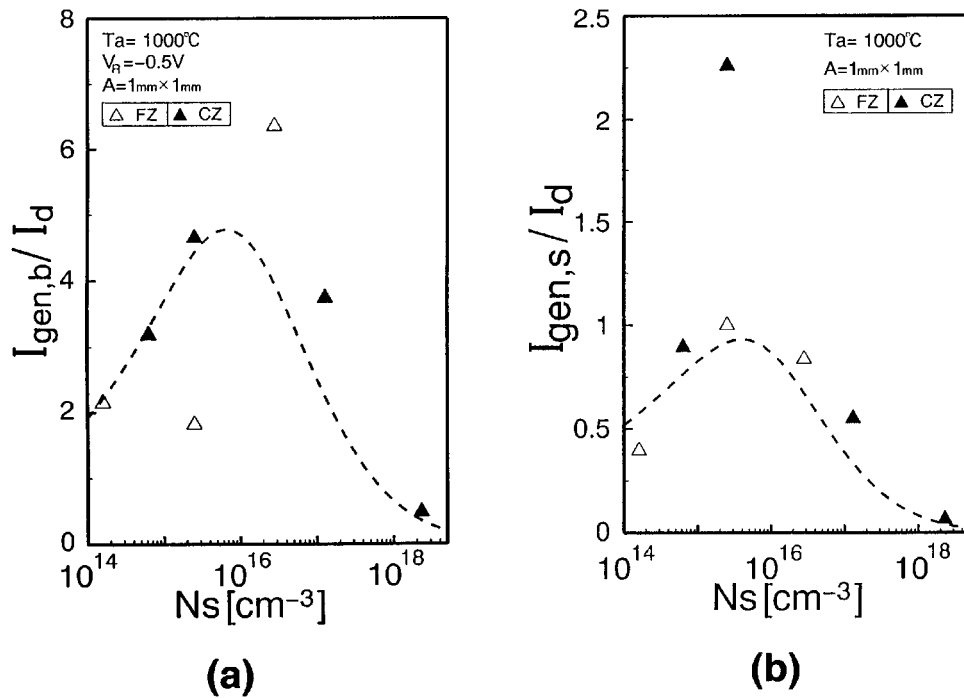


FIG. 21. (a) The ratio of the bulk generation current to the diffusion current as a function of  $N_s$  ( $1 \times 1$  mm<sup>2</sup> junctions). (b) The ratio of the surface generation current to the diffusion current as a function of  $N_s$  ( $1 \times 1$  mm<sup>2</sup> junctions).

$I_{\text{gen},b}$ , and the resulting  $I_{\text{gen}}/I_d$  and  $I_{\text{gen},b}/I_d$  ratios, as well as  $n$  and  $m$  are all function of  $|E_t - E_i|$  and  $N_t$  which were in turn found experimentally to be dependent on  $N_s$ . As a starting point for the discussion it is recalled that all the formulas presented in Sec. II assumed as a simplifying assumption that in the bulk only one energy level ( $E_t$ ) exists within the band gap. The real situation however is that there are several levels distributed within the band gap, each of them contributing to the generation/recombination process according to

its position within the band gap [Eq. (2)].  $E_t$  in this case only symbolizes an “effective” or “equivalent” value which represent the weighted influence of all these energy levels. The  $|E_t - E_i|$ ,  $N_s$  relation (Fig. 18) is determined by an interplay among three main sources of energy levels. The first is the existence of initial energy levels within the substrate itself, prior to device processing. The second is the unintentional introduction of energy levels by the addition of undesired foreign atoms contamination during processing to the active parts of the junction. Finally, the introduction of energy levels by the junction fabrication process itself (ion implantation, diffusion, etc), its parameters (implantation energy, diffusion temperature, etc), and its quality. The overall behavior of the junction performance depends on the relative contribution of the above sources through  $|E_t - E_i|$ ,  $N_t$ ,  $|E_{st} - E_{si}|$ , and  $N_{st}$ . The contribution of each source and its possible correlation with  $N_s$  is now discussed.

The initially existing energy levels within the substrate prior to device fabrication are formed mainly by undesired foreign atoms, the dominant being heavy metals, which constitute energy levels near  $E_i$ , energy levels produced by inherent crystal defects, and energy levels induced by the existing substrate dopant atoms themselves, apart from the acceptor level. The latter are responsible for part of the  $N_s$  dependence of  $|E_t - E_i|$ . The exact mechanism of formation of the dopant related energy levels is not clear, however two possible mechanisms are speculated for their formation. One is the small amount of local stress caused by the misfit in the covalent radii of the Si and the substrate dopant (B) atoms. Once this stress is above a critical value, an interaction with some extended defect (dislocation, oxide precipitate) is developed and hence an energy level results. The existence of

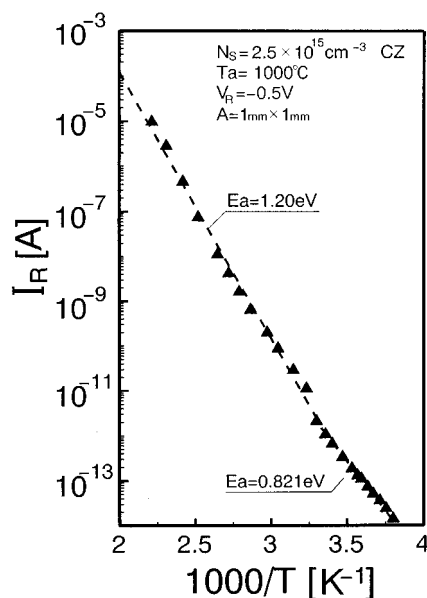


FIG. 22. The reverse current as a function of  $1000/T$  of the  $N_s = 2.5 \times 10^{15}$  cm<sup>-3</sup> Cz substrate ( $1 \times 1$  mm<sup>2</sup> junctions).

defect levels in Czochralski grown silicon due to oxide precipitates, and their relation to prior thermal history have been shown.<sup>16,41–43</sup> Their intentional formation has been demonstrated as well.<sup>44</sup> The added stress  $\sigma_1$  caused by the dopants is directly proportional to their concentration<sup>45</sup> (see the Appendix) a fact that is well correlated with the  $N_s$  dependence of  $N_t$  [Eq. (10)]. The other mechanism, is a possible weakening of the bonds between the host Si atoms caused by the dopant (B) atoms, due to the difference in their valence electrons. It is speculated that electron leaving the Si–Si covalent bond to fill the empty B–Si bond cause weakening of the neighboring Si–Si bonds. This can also induce interaction with extended defects. Both mechanisms are dopant concentration dependent. In addition, the substrate contains dopant atoms hosting lattice sites, that possess local stress (or bond weakening), resulting from the above mechanisms, which are not yet enough to create or interact with extended defects and form energy levels. Statistically, however, some of these sites bear the potential of creating recombination centers by such an interaction once enough energy is added to them. This will be referred as an “activation.” Their concentration is also  $N_s$  dependent. In the following, they will be referred to as the “weak sites.”

The merit of the ultraclean technology used here is that the second source, namely, the introduction of new energy levels near  $E_i$  to the junction during device fabrication is *almost eliminated*, due to the marked reduction of foreign atoms originated within the fabrication facility, as described in Sec. III. As a result, the main cause for the deviation of  $E_t$  from  $E_i$  is the *different nature and density* of the initially existing (mainly those close to  $E_i$ ) energy levels and newly induced energy levels by the ion implantation irradiation, which are far from  $E_i$ . This is an important point with respect to other processing technologies, that do introduce deep levels through the unintentional introduction of unwanted heavy metals atoms to the junction during processing. In that case, the density of the energy levels near  $E_i$  increases due to the additive nature of the process, and they become the dominant ones for the overall bulk generation/recombination process. As mentioned, this is largely eliminated in the present case. The increase in  $|E_t - E_i|$  with  $N_s$  in our case occurs due to the residual vacancies or divacancies<sup>46</sup> created by the implantation, left after annealing, which rapidly develop into complex lattice defects, and act as recombination centers, and due to the “activation” of some of the “weak sites” by the irradiation. These newly induced energy levels contain, accordingly, an inherent  $N_s$  dependent component. They are far from  $E_i$ , and due to their large density (with respect to the initially existing ones) become increasingly dominant. As a result the balance is now gradually shifted towards the capturing of more and more carriers in the newly added levels as  $N_s$  increases. This is expressed in the experimental results as a deviation of  $E_t$  from  $E_i$  (Fig. 18).

The addition of the newly introduced energy levels with higher  $|E_t - E_i|$  causes a decrease in the generation/recombination rate [Eq. (2)] and an increase in the generation lifetime,  $\tau_{\text{gen}}$ , with  $N_s$  [Fig. 17(a)]. This is essentially expressed in Eq. 7(a). Note, that this equation indicates that  $\tau_{\text{gen}}$

is determined by two opposing trends, since as  $N_t$  increase with  $N_s$ ,  $\tau_{\text{gen}}$  tends to decrease, however,  $|E_t - E_i|$  is the dominating factor in this case causing an overall increase in  $\tau_{\text{gen}}$  with  $N_s$ . Examining for example the junction made in the  $2.8 \times 10^{16} \text{ cm}^{-3}$  substrate, which is a representative one for IC circuits, show that for  $E_t = E_i$  case  $\tau_{\text{gen}} = \tau_n = 4.95 \times 10^{-6} \text{ s}$ . Since however in this case  $|E_t - E_i| = 0.168 \text{ eV}$ ,  $\tau_{\text{gen}}$  increases to  $1.67 \times 10^{-3} \text{ s}$ . This in turn will be shown to decrease  $I_{\text{gen},b}$  for this substrate junction, as happens for all the other junctions with varying  $N_s$  [Fig. 14(b)]. This reduction in  $I_{\text{gen},b}$  with  $N_s$  comes in addition to its reduction by  $N_s$  through  $W_R$  [Eq. 7(b)], as implied by the slope of Fig. 14(b).

Similar arguments can be made for results obtained for the surface behavior. The trend reversal of the surface recombination velocity in our data (Fig. 13) in comparison to earlier data<sup>11</sup> can be correlated to the ultraclean technology used, by the aid of Eqs. 8(c) and 8(d). The earlier data cited dealt with diffused junctions where  $E_t = E_i$  and  $E_{st} = E_{si}$  situation existed as indicated by the authors. This means  $s = s_0$  situation for these junctions. Unlike the values of  $N_t$  in the bulk,  $N_{st}$  on the surface could not be obtained from our data. Assuming however that like  $N_t$  in the bulk,  $N_{st}$  increases as well with  $N_s$ , this can explain the fact that the surface recombination rate in the earlier data<sup>11</sup> exhibited an increasing trend with  $N_s$  [Eq. 8(d)] since  $s_0$  is directly proportional to  $N_{st}$ . The reduction of the surface recombination velocity as a function of  $N_s$  (Fig. 13) in our case can be explained assuming that similarly to the bulk,  $|E_{st} - E_{si}|$  increases as well with  $N_s$ . According to Eq. 8(c) this can cause a trend reversal of  $s$  in the case where the denominator increases much faster with  $N_s$  than the numerator. This in turn explains the reduction of  $I_{\text{gen},s}$  (Fig. 12) with  $N_s$ , with relation to Eq. 8(a). The slope of Fig. 12 indicates that this reduction comes in addition to its reduction by  $A_s$ , as a function of  $N_s$ .

The results show (Fig. 20) that  $I_{\text{gen}}/I_d$  ratios, obtained for these junctions, range from values close to unity, up to about 7, at the maximum point. These significantly small ratios (with respect to ratios of tens to hundreds for junctions with  $E_t = E_{st} = E_i$ ) originate from the fact that  $I_d$  and  $I_{\text{gen}}$  are dependent in a different fashion on their respective lifetimes  $\tau_n$ ,  $\tau_{\text{gen}}$ , and  $s$ . While  $\tau_n$  practically depend only on  $N_t$  [Eq. (4)] and its dependence on  $E_t$  is negligible [ $N_A \gg n_i \exp[|E_t - E_i|/kT]$ , or  $|E_i - E_F| > |E_i - E_t|$ , see Figs. 19(a) and 19(b)],  $\tau_{\text{gen}}$  and  $s$  on the other hand are dependent on  $N_t$  and  $N_{st}$ , respectively, and dominantly on  $|E_t - E_i|$  and  $|E_{st} - E_{si}|$ , respectively. Accordingly, from Eq. 13(b) and Eq. 9(a), it is evident that the  $I_{\text{gen}}/I_d$  ratio is sensitive to  $|E_t - E_i|$  and  $|E_{st} - E_{si}|$  variations. Examine again for example, the junction produced on the  $2.8 \times 10^{16} \text{ cm}^{-3}$  substrate, with  $|E_t - E_i| = 0.168 \text{ eV}$  and  $I_{\text{gen}}/I_d = 7.2$  (Figs. 18 and 20, respectively). This ratio is composed of  $I_{\text{gen},b}/I_d$  [Fig. 21(a)] and  $I_{\text{gen},s}/I_d$  [Fig. 21(b)]. Since the first ratio is the dominant, it is enough to examine it in order to characterize  $I_{\text{gen}}/I_d$  for this substrate. From about 6.3 this ratio increases drastically by factor of 337–2022 if  $E_t = E_i$  situation would exist, increasing  $I_{\text{gen}}/I_d$  accordingly. Therefore  $I_{\text{gen}}/I_d$  can be regarded as a “figure of merit” for dc junction quality, in cases where  $|E_i - E_F| > |E_i - E_t|$  condition exists. This

point will be further addressed in the Sec. VI. The advantage of this figure of merit is that it produces a number, rather than referring to a “low reverse current,” and that it is easy to determine by simple dc measurements. It also provides a real indication for process “cleanness.” Finally, the low  $I_{\text{gen}}/I_d$  ratios mean that for these junctions,  $\tau_{\text{gen}}$  cannot be calculated directly from  $I_R$  as is routinely done<sup>1</sup> in the case where  $E_t = E_i$  or  $E_t$  is close to  $E_i$  (and hence  $I_{\text{gen}} \gg I_d$ ) or by neglecting the surface current. Instead,  $\tau_{\text{gen}}$  should be calculated from  $I_{\text{gen},b}$ , which is found by first obtaining  $I_d$  from the  $n=1$  region (taking into account the  $R_s$  effects) and subtracting it from  $I_R$  in order to find  $I_{\text{gen}}$ . Then  $I_{\text{gen},b}$  should be found by subtracting  $I_{\text{gen},s}$  from  $I_{\text{gen}}$ .  $\tau_{\text{gen}}$  is then calculated from  $I_{\text{gen},b}$ . This is specially true, according to Figs. 20 and 21(a), for low and high substrate concentrations junctions, where these ratios are particularly low.

The dependence of  $N_t$  on  $N_s$  given in Eq. (10) for As irradiation of B-doped silicon in this case is similar to the  $N_t$  dependence resulting by high energy electron and  $\gamma$ -ray irradiation of silicon.<sup>47,48</sup> This dependence led in both cases to the same dependence of minority carrier lifetime, as in Eq. (11). This indicates that high energy irradiation of Si, in general, creates defects which lead to the reduction of carrier lifetime in the form of Eq. (11). While the form of Eq. (11) is general and routinely used for lifetime characterization, the process parameters, such as implantation energy irradiation, and annealing temperature, determine the magnitude of the newly added recombination centers concentration with conjunction to  $N_s$ . This is expressed by the constant  $B(=dN_t/dN_s)$  as well as  $\tau_{ni}$ , which are process dependent parameters.<sup>17,18</sup> The creation of these levels does not automatically imply that all of them participate in the recombination process, but only a fraction of them, which increases with  $N_s$ . An explanation of the lifetime dependence of minority carriers in the neutral parts of the junction on doping concentration was given by Meier *et al.*<sup>16</sup> through the Fermi level position. It is based on the fact that not all the energy levels but only those which are filled with majority carriers can contribute to the recombination process with minority carriers under certain conditions.<sup>16</sup> As  $N_s$  increases, the Fermi level moves towards the majority carrier band edge (valence band in our case). This opens a “window” with a width of  $2|E_F - E_i|$  which includes larger fraction of the existing energy levels which are filled with majority carriers, increasing the recombination rate and accordingly decreasing the minority carrier lifetime. This situation is essentially expressed in this work by the condition  $|E_i - E_F| > |E_i - E_t|$  given in Fig. 19(b), which means that in the junctions under discussion  $\tau_n$  is dependent on  $E_F$  and not on  $E_t$ , as previously mentioned.

As pointed earlier, Eq. (11) provides the lifetime due to phonon assisted recombination process. It does not include the Auger recombination process, which may exist in the vicinity of  $2.3 \times 10^{18} \text{ cm}^{-3}$  substrate concentration. This can introduce some error that will be addressed later on. However, it should be emphasized that its existence or nonexistence is *irrelevant* as far as the bulk generation parameters are concerned, namely,  $I_{\text{gen},b}$  and  $\tau_{\text{gen}}$ . This is because both are depletion region parameters, and accordingly, require only

the phonon assisted lifetime for their determination, as seen from Eqs. (6) and (7), which were derived from Eq. (2). As a result, if the minority carrier lifetime in the neutral parts of the junction is determined, say, by a measurement that indicates that Auger recombination process component exists (at the high doping concentrations, of about  $10^{18} \text{ cm}^{-3}$  or greater), then it would be necessary to resolve from the measured data the phonon assisted component of the lifetime for the determination of  $\tau_{\text{gen}}$  and  $I_{\text{gen},b}$ . Accordingly, the value of  $\tau_n$  obtained for the  $2.3 \times 10^{18} \text{ cm}^{-3}$  junction is the correct one as far as  $\tau_{\text{gen}}$  and  $I_{\text{gen},b}$  are concerned. However, its value might be larger, as far as the diffusion current  $I_d$  is concerned, for the same junction, if Auger process exists, since  $1/\tau = 1/\tau_n + 1/\tau_A$ , where  $\tau_A$  is the lifetime due to the Auger process. Accordingly, the values inferred from  $\tau_n$  for the diffusion current components calculated for this junction in Figs. 20 and 21(a) for fitting purpose are left in the figures in order to indicate the general trend only.

Two final points regarding  $N_t$  and  $E_t$  should be noted. The first is what, at the first glance, may be seen as a “paradox.” It is noted from the experimental results that as  $N_t$  increases (with  $N_s$ ) the recombination/generation rate decreases as seen by  $I_{\text{gen},b}$  and  $\tau_{\text{gen}}$ , while one would expect the opposite. The solution to the “paradox” is that  $U$  [Eq. (2)] is determined simultaneously by both  $N_t$  and  $E_t$ , the latter being the dominant one. While  $U$  is linearly dependent on  $N_t$ , it is inversely dependent on  $\exp(E_t - E_i)$ , which in our junction cause an overall reduction in  $U$  as  $N_s$  increases, despite the fact that  $N_t$  increases. This might be explained as follows: as  $N_s$  increases,  $N_t$  increases as well [Eq. (10)] and the number of generation/recombination events increase, but due to the position of  $E_t$ , which becomes far from  $E_i$ , the carriers are trapped for shorter time, and then released to the bands, giving rise to larger  $\tau_{\text{gen}}$ , and thus decreasing the recombination rate,  $U$ . The second point regarding  $N_t$  and  $E_t$  is that in Eq. (2) and in the following equations, all the recombination centers ( $N_t$ ) are assumed to be evenly distributed in the crystal volume, an assumption which is probably correct in the substrate within reasonable limits, before processing. The real situation within the active parts of the  $n^+p$  junctions under discussion, however, is different since  $N_t$  is not constant (specifically within the depletion region) and deviates by a magnitude which depends on the implantation/annealing parameters in conjunction with  $N_s$ . According to Eq. (10) it can be expected that the recombination/generation centers distribution has a profile which is related to the doping profile in both junction sides. This means that  $N_t$  and  $E_t$  are different not only from junction to junction as a function of  $N_s$ , but vary also within each junction. This fact bear two results. The first that like  $E_t$ ,  $N_t$  in the equations used, is some “effective” or some weighted average value. The second is that the results obtained for  $N_t$  and  $E_t$  are dependent on the magnitude and polarity of junction bias. This is because a change in bias results in a change in  $W$  which may include higher or lower values of  $N_t$  and  $E_t$  depending on the direction and magnitude of the change. Therefore, when providing numbers for  $N_t$  and  $|E_t - E_i|$ , the experimental conditions (bias) should be specified. The effect of the above will

somewhat affect the magnitude of  $N_t$  and  $|E_t - E_i|$ , but not their trends with  $N_s$ .

The increase in  $N_t$  with  $N_s$ , can also explain the drastic fall in  $R_p$  in Fig. 7, as  $N_s$  exceeds some critical concentration. The equivalent circuit used for deriving Eq. (14), includes  $R_p$  directly parallel to the ideal junction. Therefore  $R_p$  in this case does not include any bulk or contact properties related to  $R_s$  but it does provide a measure of the ohmic behavior of the depletion region. In the fitting process,  $R_p$  is mainly determined by the computer program from the lower current region of the  $I$ - $V$  characteristics which overlap part of the  $I$ - $V$  region for the simultaneous determination of  $I_{gf}$ .  $I_{gf}$  is created by the action of discrete recombination centers, which are distinctly separated from each other, and have no "coupling" between them. They trap and emit carriers from and to the respective bands, and as such, their action represent *electronic activities*, which is manifested by  $I_{gf}$ . As  $N_t$  increases above a certain value, some of the defects possibly together with others which were electronically inactive at low doping concentrations, may form a path through which the carriers are moving from one center to another and not through the bands. These current "channels" represent an *ohmic* current component  $I_\Omega$ , which is manifested by the fall in  $R_p$  and represent an *electrical activity* which means loss, in this case. It is not clear if the path is continuous, or if some "jumping" mechanism of carriers exists between some "islands" of defects in the path. In any case, the value of the critical point for  $R_p$  drastic reduction, in Fig. 7 (at  $N_s \geq 2.5 \times 10^{15} \text{ cm}^{-3}$ ), depend on the technological process which introduces the defects and determine their properties. These depletion region currents, namely  $I_\Omega$ ,  $I_{gf}$ , and the diffusion current  $I_d$ , are comparable in their values, in the low  $R_p$  regime ( $N_s > 2.5 \times 10^{15} \text{ cm}^{-3}$ ) of Fig. 7. Accordingly, neglecting  $R_p$  from the equivalent circuit in this regime will result in an error in the determination of the values of  $I_d$  and even more in  $I_{gf}$ . It is noted that at the same time,  $R_s$  (Fig. 6) is decreasing monotonically with  $N_s$ , in contrast to the drastic fall in  $R_p$ . This is due to the different mechanisms of current transport within the low and high field regions. Defects in the neutral bulk region have much weaker effect on the resistance, which is mainly determined by dopant concentration. The drastic fall of  $R_p$  on the other hand, is defect dominated, rather than  $N_s$ .

## VI. CONCLUSION

Using ultraclean process technology and the related suppression of unintentional introduction of heavy metal atoms, as well as other contaminants to the active parts of the junction was shown to cause a principal change in junction behavior resulting marked improvements in its dc performance quality. It is concluded that this is achieved by altering the recombination process itself, which results from a shift of  $E_t$  from  $E_i$ . This shift is shown to be dependent on  $N_s$ , and as such, enables one to control the marked increase in  $\tau_{\text{gen}}$ , and the parallel reduction in  $I_{\text{gen}}$ , and  $I_{\text{gen}}/I_d$  ratios. The  $|E_t - E_i|$ ,  $N_s$  relation can therefore be used for device design considerations. This is in contrast to the previous situation where  $I_{\text{gen}}$  as well as other generation parameters were largely determined by parasitic effects.

From Fig. 20 it is seen that low values of  $I_{\text{gen}}/I_d$  can be attained for both low and high  $N_s$  values. Generally speaking, from the point of view of low  $I_{\text{gen}}/I_d$  considerations, it seems more desirable to choose high  $N_s$  values because in such a case both  $I_{\text{gen}}$  and  $I_d$  are low [Figs. 14(a) and 3, respectively] in addition to their low ratio. Obviously, the doping concentrations are determined by other device performance requirements as well. However, a situation may arise, that in future ULSI devices design considerations, a tendency towards choosing high  $N_s$  values may be preferred, if related low temperature annealing problems will be solved. This is due to several reasons, some of which are outlined here. The reduction in junction area will result in an increased  $R_s$ , and the increased  $N_s$ , with conjunction to other structural parameters, can alleviate this problem. In addition, high  $N_s$  may reduce surface inversion problems to a degree that might eliminate guarding, altogether, increasing device packaging density. Finally, the scaling down is accompanied by a significant reduction in operation currents, and therefore necessitate a parallel reduction in noise levels, to ensure reasonable signal to noise ratios and reduce information errors. Since noise level is directly proportional to  $I_R$ , choosing high  $N_s$  values, where  $I_R$  is small (Fig. 2), is a viable solution.

The value of  $\tau_n$  was determined to be  $1/\sigma v_{\text{th}} N_t$  for our junctions, under the condition that  $|E_i - E_F| > |E_t - E_i|$ , which was shown to prevail for this case. If, however, in the future, better substrate quality with greatly suppressed (or eliminated) heavy metal atom content will be realized, the above inequality may be reversed. This can cause three results: an increase of minority carrier lifetime ( $\tau_n > 1/\sigma v_{\text{th}} N_t$ ) according to Eq. (2) in the junction neutral zones, as a function of the deviation of  $E_t$  from  $E_i$  (similarly to  $\tau_{\text{gen}}$ ). Secondly, an improvement in  $I_d$ , which will be decreased as a result of increased  $\tau_n$ , although in a less drastic fashion than  $I_{\text{gen},b}$  (and hence  $I_{\text{gen}}$ ). This is because  $I_{\text{gen},b}$  is inversely proportional to  $\tau_{\text{gen}}$ , while  $I_d$  is inversely proportional to  $\tau_n^{1/2}$ . As a result, the sensitivity of  $I_{\text{gen}}/I_d$  ratio to  $|E_t - E_i|$  will decrease, a fact that will stabilize its value against the influence of the above mentioned parasitic effects. In any case, the simultaneous reduction in both  $I_{\text{gen}}$  and  $I_d$  as a function of  $|E_t - E_i|$ , will further reduce  $I_R$ , improving dc junction performance quality. As a paradox, it should be noted that the  $I_{\text{gen}}/I_d$  ratios might increase in such a case (namely, if  $|E_i - E_F| < |E_t - E_i|$ ), despite the reduction in  $I_R$ . Therefore, the  $I_{\text{gen}}/I_d$  ratio can serve as a figure of merit for  $|E_i - E_F| > |E_t - E_i|$  situation only, which, at present, was experimentally shown to be a realistic situation.

## VII. SUMMARY

It was experimentally demonstrated that the suppression of the introduction of undesired heavy metal atoms and other contaminations to the active parts of ion implanted  $n^+p$  junctions during device processing, results in significant improvement in the junction quality, mainly through the generation parameters, namely,  $I_{\text{gen}}$ ,  $\tau_{\text{gen}}$ ,  $n$ , and  $m$ . It is concluded that these improvements are result of the deviation of  $E_t$  from  $E_i$ , and  $E_{st}$  from  $E_{si}$  which were found to increase with  $N_s$ . Under the ultraclean processing technology used



here, the number of new energy levels introduced near  $E_i$  during processing is minimized. Accordingly, the above deviation of  $E_t$  and  $E_{st}$  is dominantly a result of a balance between initially existing energy levels in the substrate prior to processing (with mainly  $E_t$  close to  $E_i$  levels) and newly created energy levels by the implantation irradiation and post-annealing, both having an  $N_s$  dependent component. These new energy levels are far from  $E_i(E_{st})$ , and due to their high density which increase with  $N_s$ , cause the above deviation.  $I_{gen}/I_d$  ratios were found to be extremely small, with respect to their values in the  $E_t = E_i$  case, due to the fact that while  $I_{gen,b}$  is dependent on both  $N_t$  and  $E_t$ ,  $I_d$  in these junctions is practically dependent only on  $N_t$ . The above approach can, under these fabrication conditions, obtain better quality control for device performance. It was accordingly proposed that the criteria for quality determination will be defined as  $I_{gen}/I_d$ , which serves as a figure of merit for dc junction performance.

## ACKNOWLEDGMENT

This work was carried out in the Super Clean Room of the Laboratory for Electronic Intelligent Systems, Research Institute of Electrical Communication, Tohoku University, Japan.

## APPENDIX: IMPURITY RELATED STRESS

The reduction in lifetime [Eq. (11)] with  $N_s (=N_A)$  was related to the increase in  $N_t$  [Eq. (10)]:

$$N_t = N_{ti} + BN_s \quad (A1)$$

The second term in Eq. (A1) represents the *added trapping centers* due to the presence of dopants. A possible mechanism for the formation of the trapping centers is a local stress  $\sigma_1$  [dyne/cm<sup>2</sup>] in a lattice site that host an impurity atom. This stress develops due to the misfit in the covalent radii of the Si atoms ( $r_{Si}=0.104$  nm) and the Boron atoms ( $r_B=0.088$  nm),<sup>49</sup> and its value is calculated by:<sup>45</sup>

$$\sigma_1 = \left[ 1 - \left( \frac{r_d}{r_{Si}} \right)^3 \right] \left( \frac{N_s}{N_{Si}} \right) \frac{Y_1}{1-P}, \quad (A2)$$

where  $Y_1$  is the Young's modules ( $1.31 \times 10^{11}$  dyne/cm<sup>2</sup>),  $P$  is the Poisson's ratio ( $-0.33$ ),  $N_{Si}$  is the concentration of silicon atoms ( $4.96 \times 10^{22}$  cm<sup>-3</sup>), which yields:

$$\sigma_1 = AN_s, \quad (A3)$$

where  $A = 7.83 \times 10^{-12}$  dyne cm. Equation (A3) shows that the *added stress* due to the presence of dopant atoms is directly proportional to their concentration, a fact that is in accordance with the second term of Eq. (A1).

<sup>1</sup> D. K. Schroder, IEEE Trans. Electron Devices **ED-29**, 1336 (1982).

<sup>2</sup> W. Shockley and W. T. Read, Phys. Rev. **87**, 835–842 (1952).

<sup>3</sup> R. N. Hall, Phys. Rev. **87**, 387 (1952).

<sup>4</sup> A. S. Grove, *Physics and Technology of Semiconductors Devices*, (Wiley, Singapore, 1967).

<sup>5</sup> C. T. Sah, R. N. Noyce, and W. Shockley, Proc. IRE **45**, 1228 (1957).

<sup>6</sup> S. M. Sze, *Physics of Semiconductor Devices*, 2nd ed. (Wiley, Singapore, 1981).

<sup>7</sup> M. V. Whelan, Solid-State Electron. **12**, 963 (1969).

<sup>8</sup> J. Cornu, R. Sittig, and W. Zimmermann, Solid-State Electron. **17**, 1099 (1974).

<sup>9</sup> S. K. Ghandi, *Semiconductor Power Devices* (Wiley, New York, 1977).

<sup>10</sup> A. S. Grove and D. J. Fitzgerald, Solid-State Electron. **783–806**, 1966.

<sup>11</sup> D. J. Fitzgerald and A. S. Grove, Surf. Sci. **9**, 347 (1968).

<sup>12</sup> D. B. M. Klaassen, Solid State Electron. **35**, 961 (1992).

<sup>13</sup> J. G. Fossum, R. P. Mertens, D. S. Lee, and J. F. Nijs, Solid State Electron. **26**, 569 (1983).

<sup>14</sup> M. S. Tyagi and R. Van Overstraten, Solid State Electron. **26**, 577 (1983).

<sup>15</sup> H. S. Bennet, Solid State Electron. **27**, 893 (1984).

<sup>16</sup> D. H. Meier, J. O. Hwang, and R. B. Campbell, IEEE Trans. Electron Devices **ED-35**, 70 (1988).

<sup>17</sup> D. J. Roulstone, N. D. Arora, and S. G. Chamberlaine, IEEE Trans. Electron Devices **ED-29**, 284 (1982).

<sup>18</sup> S. Bellone, G. Busatto, and C. M. Ransom, IEEE Trans. Electron Devices **ED-8**, 532 (1991).

<sup>19</sup> H. S. Bennett, IEEE Trans. Electron Devices **ED-30**, 920 (1983).

<sup>20</sup> A. Neugroschel, F. A. Lindholm, and C. T. Sha, IEEE Trans. Electron Devices **ED-24**, 662 (1977).

<sup>21</sup> T. Ohmi, N. Mikoshiba, and K. Tsubouchi, *ULSI Science and Technology/1987*, edited by S. Broydo, and C. M. Osburn (The Electrochemical Society, Pennington, 1988), pp. 761–85.

<sup>22</sup> T. Ohmi, Microcontamination **6**, 49 (1988).

<sup>23</sup> K. Sugiyama and T. Ohmi, Microcontamination **6**, 49 (1988).

<sup>24</sup> Y. Kanno and T. Ohmi, Microcontamination **6**, 23 (1988).

<sup>25</sup> K. Sugiyama, T. Ohmi, T. Okumura, and F. Nakahara, Microcontamination **7**, 37 (1989).

<sup>26</sup> K. Sugiyama, F. Nakahara, and T. Ohmi, Microcontamination **7**, 29 (1989).

<sup>27</sup> K. Sugiyama, T. Ohmi, Y. Mizoguchi, and F. Nakahara, *Automated Integrated Circuits Manufacturing*, edited by V. Akins (The Electrochemical Society, Pennington, 1990), Vol. PV90-3, pp. 148–172.

<sup>28</sup> K. Yabe, Y. Motomura, H. Ishikawa, T. Mizuniwa, and T. Ohmi, Microcontamination **7**, 37 (1989).

<sup>29</sup> T. Ohmi, and M. Yasuda, Microcontamination **7**, 23 (1989).

<sup>30</sup> T. Ohmi, H. Inaba, and T. Takenami, Microcontamination **7**, 29 (1989).

<sup>31</sup> T. Ohmi, H. Inaba, and T. Takenami, Microcontamination **7**, 29 (1989).

<sup>32</sup> T. Ohmi and N. Mikoshiba, in Proceedings of the First International Symposium on ULSI Science and Technology, Philadelphia, 1987, Abst. No. 212.

<sup>33</sup> T. Ohmi, K. Masuda, T. Hashimoto, T. Shibata, M. Kato, and Y. Ishihara, in Extended Abstracts of the Conference on Solid State Devices and Materials, Tokyo, 1987, pp. 299–302.

<sup>34</sup> T. Nitta, T. Ohmi, Y. Ishihara, A. Okita, T. Shibata, J. Sugiura, and N. Ohwada, J. Appl. Phys. **67**, 7404 (1990).

<sup>35</sup> T. Ohmi, M. Onodera, G. Sato, T. Shibata, and M. Morita, in Extended Abstracts of the Electrochemical Society Fall Meeting, Chicago, 1988, pp. 596–597.

<sup>36</sup> K. Tomita, T. Migita, S. Shimonishi, T. Shibata, T. Ohmi, and T. Nitta, J. Electrochem. Soc. **142**, 1692 (1995).

<sup>37</sup> H. Aharoni, T. Ohmi, M. M. Oka, A. Nakada, and Y. Tama (to be published).

<sup>38</sup> K. Ohyu, A. Hiraiwa, T. Itoga, J. Yugami, and M. Ohkurai, in Proceedings of the Symposium on ULSI Ultra Clean Technology, Tokyo, Japan, 1994, pp. 356–364.

<sup>39</sup> M. Horiuchi and K. Ohyu, IEEE Trans. Electron Devices **42**, 876 (1995).

<sup>40</sup> K. Ohyu, M. Hiraiwa, and K. Watanabe, IEEE Trans. Electron Devices **42**, 1404 (1995).

<sup>41</sup> J. M. Hwang and D. K. Schroder, J. Appl. Phys. **59**, 2476 (1986).

<sup>42</sup> J. Hwang, D. K. Schroder, and A. M. Goodman, IEEE Electron Device Lett. **EDL-7**, 172 (1986).

<sup>43</sup> A. Bourret, J. Thibault-Desseaux, and D. N. Seidman, J. Appl. Phys. **55**, 825 (1984).

<sup>44</sup> H. Holzlein, G. Pensl, M. Schulz, and N. M. Johnson, Appl. Phys. Lett. **48**, 916 (1986).

<sup>45</sup> H. F. Wolf, *Semiconductors* (Wiley-Interscience, New York, 1971).

<sup>46</sup> S. K. Ghandi, *VLSI Fabrication Principles* (Wiley, New York, 1994).

<sup>47</sup> G. K. Wertheim, Phys. Rev. **105**, 1730 (1957).

<sup>48</sup> P. V. Kuchinski and V. M. Lomako, Solid State Electron. **29**, 1041 (1986).

<sup>49</sup> C. Kittel, *Introduction to Solid State Physics*, 6th ed. (Wiley, New York, 1986).